



Cu(II)-baicalein enhance paracrine effect and regenerative function of stem cells in patients with diabetes

Kaijing Liu^{a,#}, Ruihao Li^{e,f,#}, Shusen Wang^{c,d}, Xue Fu^a, Ni Zhu^a, Xiaoyu Liang^a, Huiyang Li^a, Xiaoli Wang^{a,**,1}, Le Wang^{c,d,***,1}, Yongjun Li^{e,f,****,1}, Jianwu Dai^a, Jing Yang^{a,b,1,*}

^a Key Laboratory of Advanced Medical Materials and Devices, Institute of Biomedical Engineering, Tianjin Institutes of Health Science, Chinese Academy of Medical Science & Peking Union Medical College, Tianjin, 300192, China

^b Tianjin Medical Health Research Institute, Tianjin, 300192, China

^c Organ Transplant Center, Tianjin First Central Hospital, Nankai University, Tianjin, China

^d Tianjin Clinical Research Center for Organ Transplantation, Tianjin, China

^e Department of Vascular Surgery, Beijing Hospital, National Center of Gerontology, Institute of Geriatric Medicine, Chinese Academy of Medical Science & Peking Union Medical College, Beijing, 100730, China

^f Graduate School of Peking Union Medical College, Beijing, 100730, China

ARTICLE INFO

Keywords:

Angiogenesis
Adipose stem cells
Type 1 diabetes mellitus
Paracrine effect
Regenerative function

ABSTRACT

The development of engineered or modified autologous stem cells is an effective strategy to improve the efficacy of stem cell therapy. In this study, the stemness and functionality of adipose stem cells derived from type 1 diabetic donors (T1DM-ASC) were enhanced by treatment with Cu(II)-baicalein microflowers (Cu-MON). After treatment with Cu-MON, T1DM-ASC showed enhanced expression of the genes involved in the cytokine-cytokine receptor interaction pathway and increased cytokine secretion. Among the top 13 differentially expressed genes between T1DM-ASC and Cu-MON-treated T1DM-ASC (CMTA), some genes were also expressed in HUVEC, Myoblast, Myofibroblast, and Vascular Smooth Muscle cells, inferring the common role of these cell types. In vivo experiments showed that CMTA had the same therapeutic effect as adipose-derived stem cells from non-diabetic donors (ND-ASC) at a 15% cell dose, greatly reducing the treatment cost. Taken together, these findings suggest that Cu-MON promoted angiogenesis by promoting the stemness and functionality of T1DM-ASC and influencing multiple overall repair processes, including paracrine effects.

1. Introduction

Stem cell therapy has been applied in many fields, such as those for diabetes mellitus [1], spinal cord injury [2], leukemia [3], and tissue engineering [4], bringing new hope for patients [5]. However, clinical studies have found that the reduced viability after stem cell

transplantation makes stem cell therapy less effective than desired [6,7]. All these factors are mainly due to various factors affecting the cell fate after cell transplantation, including inappropriate physical, chemical, and biological stimulation during the cell culture period, mechanical damage during cell transplantation, and a pathological oxidative and inflammatory microenvironment after cell transplantation. These

Peer review under responsibility of KeAi Communications Co., Ltd.

* Corresponding author. Key Laboratory of Advanced Medical Materials and Devices, Institute of Biomedical Engineering, Tianjin Institutes of Health Science, Chinese Academy of Medical Science & Peking Union Medical College, Tianjin, 300192, China.

** Corresponding author.

*** Corresponding author. Organ Transplant Center, Tianjin First Central Hospital, Nankai University, Tianjin, China.

**** Corresponding author. Department of Vascular Surgery, Beijing Hospital, National Center of Gerontology, Institute of Geriatric Medicine, Chinese Academy of Medical Science & Peking Union Medical College, Beijing, 100730, China.

E-mail addresses: wangxl@bme.pumc.edu.cn (X. Wang), wangle_nancy@163.com (L. Wang), liyongjun4679@bjhmoh.cn (Y. Li), yangjing@bme.cams.cn, yangjing37@hotmail.com (J. Yang).

These authors contribute equally to this work.

¹ Present Addresses: Key Laboratory of Advanced Medical Materials and Devices, Institute of Biomedical Engineering, Tianjin Institutes of Health Science, Chinese Academy of Medical Science & Peking Union Medical College, Tianjin, 300192, China

<https://doi.org/10.1016/j.bioactmat.2024.03.013>

Received 7 November 2023; Received in revised form 8 March 2024; Accepted 10 March 2024

2452-199X/© 2024 The Authors. Publishing services by Elsevier B.V. on behalf of KeAi Communications Co. Ltd. This is an open access article under the CC BY-NC-ND license (<http://creativecommons.org/licenses/by-nc-nd/4.0/>).

adverse factors even lead to rapid cell loss within a few hours after transplantation [8,9], compromising the therapeutic efficacy of transplanted stem cells.

Several methods, including hydrogels, nanodelivery systems, and gene-editing techniques, have been developed to address these problems. Surface tethering of inflammation-modulated nanostimulators to stem cells promoted vascularization of three-dimensional microvascular chips, thereby enhancing perfusion, walking, and muscle mass recovery in mice after ischemia [10]. “NO gel”, which releases NO by crosslinking glutaminase reactions, coats the stem cells and promotes the production of pericytes [11]. When the NO gel was implanted, BMSC numbers increased and the expression of pericellular markers (NG2 and CD146) and human nuclei colocalized, which led to accelerated wound healing. The stem cell delivery system with a three-dimensional (3D) cavity structure promoted the formation of cell pellets and increased the expression of therapeutic growth factors [12]. The Cas9-AAV6-based genome editing tool platform generated PDGF-BB- and VEGFA-hypersecreting hMSC lines as short-term local wound healing agents in a diabetic mouse model [13]. Overall, hydrogels, nanodelivery systems, and gene editing techniques enhanced stem cell activity at ischemic sites. However, complex preparation methods and potential immune responses after biomaterial transplantation are major challenges for clinical conversion.

Moreover, mesenchymal stem cells from bone marrow, fat, the umbilical cord, and the placenta have different advantages and disadvantages when applied to clinical studies [14]. Umbilical cord and placental mesenchymal stem cells were highly pro-angiogenic. However, their population was fixed, and their extraction was restricted. Bone marrow mesenchymal stem cells are homologous and have low immunogenicity. However, their extraction is invasive and painful to the human body, and there is a risk of infection [13]. The extraction of adipose mesenchymal stem cells was less invasive, less painful, and had a high amount of regeneration [15,16], but it was also limited by the age, gender, and physical condition of the donor [17], and is similar to those of bone marrow mesenchymal stem cells [18]. Importantly, most patients with critical limb ischemia are elderly and often have complications such as diabetes. Their tissue repair was impaired due to persistent chronic inflammation, reduced growth factor secretion, and disrupted vascularization [19,20]. In previous studies, we found that, unlike adipose-derived stem cells from non-diabetic donors (ND-ASC), adipose-derived stem cells from type 2 diabetic donors (T2DM-ASC) exhibited many defects in certain features, including cell cycle delay and multilineage differentiation [21]. Moreover, other studies have reported that the adipose-derived stem cells from type 1 diabetic donors (T1DM-ASC) proliferative response is impaired when compared to that of ND-ASC [22]. However, most studies now focus only on the use of biomaterials to enhance the homing effect [23], survival rate [24] and paracrine effects [10] of ND-ASC in ischemic sites, but ignore the use of biomaterials to regulate the T1DM-ASC fate, prompting it to a normal physiological state. To our knowledge, there is no available method for the precise control and regulation of pathological adipose-derived stem cells.

In conclusion, the use of biomaterials with excellent properties to pretreat stem cells can protect cells from adverse damage before transplantation, improve cell quality, and promote their recovery to a normal stem cell state. Not introducing biomaterials can avoid the potential immune reaction in the body, which can provide a potential therapeutic strategy for cell engineering. In our previous work, Cu-MON integrated the abilities of baicalein and copper ions to achieve redox homeostasis, inflammation inhibition, and angiogenesis promotion, and exhibited excellent capability in the treatment of critical limb ischemia with diabetes mellitus [25]. Therefore, the application of Cu-MON to improve the function of T1DM-ASC will provide new options for the use of autologous stem cells in regenerative medicine. In this study, we compared the transcript sequencing of ND-ASC from healthy individuals, T1DM-ASC from T1D patients with diabetes, and T1DM-ASC

pretreated with Cu-MON (CMTA), along with their multilineage differentiation potential, growth factor secretion, and oxidative stress levels. Cu-MON was used to promote the stemness and paracrine effects of T1DM-ASC. The physiological status of the regulated cells was assessed based on cell-to-cell interactions and transcriptome sequencing results. Furthermore, we systematically evaluated the therapeutic efficacy of inflammation, growth factor secretion, revascularization, and recovery of motor function in the CLI model of T1D mice, which may facilitate our understanding of the mechanisms and potential clinical applications of using autologous ASC to promote tissue repair in diabetes patients.

2. Methods

2.1. Cell lines and animals

Human peripancreatic adipose tissues were obtained from T1DM (n = 1) and non-diabetic organ donors (n = 2). ND-ASC and T1DM-ASC were extracted from the indicated adipose tissues according to the guideline of Declaration of Helsinki. All the experimental procedures were approved by the Ethics Committee of Tianjin First Central Hospital of Nankai University and informed consents were obtained (2017N080KY). The information of the ND and T1DM donors is available in Table 1.

Mouse macrophages RAW264.7, mouse embryonic fibroblast cells line 3T3 (NIH3T3), and human smooth muscle cells (SMC) were purchased from the Cell Bank of China Academy of Sciences. Human umbilical vein endothelial cells (HUVEC) were purchased from Procell Life Science&Technology Co., Ltd (Wuhan, China). Six-week-old male B6 mice (20 ± 2 g) were purchased from Beijing Vital River Laboratory Animal Technology Co., Ltd (Beijing, China) and housed in the Animal Facility of Institute of Radiation Medicine, Chinese Academy of Medical Sciences. All animal operations were reviewed and ethically approved by the Tianjin Committee of Use and Care of Laboratory Animals, and the overall project protocols were approved by the Animal Ethics Committee of the Chinese Academy of Medical Sciences (IRM-DWLL-2022145).

2.2. Effect of Cu-Mon on cell viability of T1DM-ASC

Briefly, T1DM-ASC was seeded in a 96-well plate with a density of 5000 cells/well. After incubation for 24 h, cells were treated with different concentration of Cu-MON (0, 3.125, 6.25, 12.5, 25, 50, 100, 200 µg mL⁻¹). At day 1, 2, 3, 10 µL of CCK-8 solution was added into each well and incubated for 1 h, and the OD value at 450 nm was measured using a microplate reader (Thermo Fisher Scientific, MA, USA). Cell viability was evaluated according to a ratio of the OD value between experimental group and control group.

Lactate dehydrogenase (LDH) assay was used to evaluate the cell membrane integrity of T1DM-ASC after incubated with Cu-MON. T1DM-ASC were seeded into 96-well plates with a cell density of 5 × 10⁴ cells mL⁻¹. After incubation for 24 h, Cu-MON (0–200 µg mL⁻¹) were added to co-incubate with cells for 24, 48, 72 h. Then the culture medium was collected, and 120 µL of the supernatant was added to 60 µL of LDH reaction solution in a 96-well plate following the manufacturer protocol. The mixture was shaken for 30 min at room temperature. To determine the amount of LDH, a Varioskan Flash microplate reader was used to measure the absorbance at 490 and 690 nm (as a reference) simultaneously. The LDH reaction solution with culture medium only (without

Table 1
Donor information.

	N (Male/Female)	Age (y)	HbA1c (%)	BMI (kg/m ²)
ND	female	31	–	20.83
ND	female	32	–	19.10
T1DM	female	31	6.3	19.53

cells) was defined as a blank control. T1DM-ASC treated with Triton X-100 was served as a positive control.

2.3. Biocompatibility in vivo

The biocompatibility of Cu-MON in normal mice was evaluated. Firstly, normal Balb/c mice ($n = 5$) were injected with saline and Cu-MON (2.5 μg , 7.5 μg , 12.5 μg and 17.5 μg) into the gastrocnemius in a scattered manner at day 1. The body weight of mice was monitored at days 1, 4, 7, 14, 21, and 28. At day 28, 500 μL of blood was collected from orbit, and serum was centrifuged to determine the levels of IL-6 and TNF- α . Then the main organs and gastrocnemius were isolated and weighed, and the organ index was calculated by the ratio of organ to body weight. The copper content in the main organs was determined by ICP-MS-QC (Thermo Fisher Scientific, USA).

2.4. Determination of cell growth curve

First, the standard curve of cell number and absorbance was prepared by double dilution methods and CCK8. The initial number of cells was 24,000 (in 96-well plates) and then double dilution for 5 times. 10 μL of CCK-8 solution was added into each well and incubated at 37 $^{\circ}\text{C}$ for 30 min, and the OD value at 450 nm was measured. Subsequently, the cells were seeded in 96-well plates with a cell density of 2400 cells/well. After 12 h serum-free culture, the culture medium was changed to full medium. And at the corresponding time point, 10 μL of CCK-8 was added, and the absorbance was detected after incubation at 37 $^{\circ}\text{C}$ for 30 min. According to the standard curve, the number of cells at each time point was calculated.

2.5. Endocytosis of T1DM-ASC on Cu-Mon

Cells were seeded in confocal dish with a cell density of 1×10^5 cells. After incubation for 24 h, Cy5-BAI, CuCl_2 , Cu-MON, Cy5-Cu-MON were added to co-incubate with cells for 4, 24, 48 h. Then cells in CuCl_2 , Cu-MON, Cy5-Cu-MON group were stained by Rhodamine B hydrazide (RB) and all cells were detected by Confocal laser scanning microscope (Olympus FV1000).

2.6. RNA extraction, sequencing and analysis

RNA extraction, library preparations and sequencing reactions were conducted at Wuhan BGI Technology Co., Ltd. (Wuhan, China). Total RNA was extracted using TRIzol reagent (Thermo Fisher Scientific, MA, USA), and each group was prepared with three parallel replicates. Extracted RNA samples were quantified using a Nano Drop (Thermo Fisher Scientific, MA, USA) and RNA integrity was checked on Agilent 2100 bioanalyzer (Thermo Fisher Scientific, MA, USA).

RNA sequencing libraries were prepared. Briefly, a certain amount of Total RNA samples were taken, digested by DNase I and purified for mRNA using Oligo (dT) magnetic beads. Purified mRNA was fragmented into small pieces with fragment buffer at appropriate temperature, and random primers were added for first-strand cDNA synthesis. Then second-strand synthesis was performed instead of dTTP with dUTP. The amplified cDNA was end-repaired, adenylated at 3' ends, and purified by Ampure XP Beads. Afterwards, the ligation products were PCR amplified after digesting the U-labeled second-strand template with UDG enzyme, and purified by Ampure XP Beads. The sequencing libraries were validated using Agilent 2100 Bioanalyzer and quantified using ABI StepOnePlus Real-Time PCR System (TaqMan Probe). Subsequently, the PCR products were denatured into single strands and circularized by the splint oligo sequence. The single strand circle DNA (ssCir DNA) was formatted as the final library. Finally, the final library was amplified with phi29 to make DNA nanoball (DNB) which had more than 300 copies of one molecular, DNBs were loaded into the patterned nanoarray and single end 50 bases reads were generated on BGISEQ-500 platform

(Wuhan, China).

Read quality was evaluated using SOAPnuke [26] (v1.5.2) and clean reads were obtained and stored in FASTQ format. The clean reads were mapped to the reference genome using HISAT2 [27] (v2.0.4). Data were processed with Ericscript [28] (v0.5.5) and rMATS [29] (V3.2.5). Gene expression was quantified with Bowtie2 [30] (v2.2.5) and RSEM (v1.2.12). The heatmap was drawn by pheatmap [29] (v1.0.8) according to the gene expression in different samples. Essentially, differential gene expression analysis was performed using DESeq2 (v1.4.5). Genes with $\log_2|\text{fold change}| \geq 1$ and $Q\text{value} \leq 0.05$ were considered statistically significant.

2.7. Quantitative real-time PCR (qRT-PCR) assay

First, ND-ASC, T1DM-ASC was seeded into a 6-well plate with a density of 5×10^5 cells per well and cultured for 24 h. Then Cu-MON (12.5 $\mu\text{g mL}^{-1}$) was added and co-incubated with T1DM-ASC for 2 d (abbreviated ad CMTA). Cell samples were homogenized in TRIzol reagent (Invitrogen), and total RNA was extracted from the tissue according to the manufacturer's protocol. cDNA synthesis was performed by utilizing degenomic retroactivation premix (GenStar, A230), Universal DNA Purification Recovery Kit (Tiangen Biotech (Beijing) Co. Ltd., DP214-03) and ZTOPO-Blunt/TA Zero-background rapid cloning kit (Beijing Zoman Biotechnology Co., Ltd., ZC211). Reverse transcriptase-polymerase chain reaction (RT-PCR) was performed by 2x M5 HiPer SYBR Premix Es Taq (Mei5 Biotechnology Co., Ltd, Beijing, China), a quantitative PCR instrument (Roche, LightCycler480) and PCR appearance (Biometra GmbH, 844-070-882). The standard curve was constructed and the mRNA expression of the indicated genes was calculated by the $2^{-\Delta\Delta\text{CT}}$ method. The Primer sequences are listed in Table 2.

2.8. Flow cytometry

Cells were blocked with 5% goat serum, incubated with Anti-PPAR- γ (1:1500 dilution, abcam, ab178860), Anti-Sox-9 (1:190 dilution, abcam, ab185230), Anti-BGLAP (1:100 dilution, PA5-78871), followed by Donkey anti-Rabbit IgG (H + L) Highly Cross-Adsorbed Secondary Antibody, Alexa Fluor™ Plus 488 (for 30 min at room temperature, 1:1000 dilution). Then the expression PPAR- γ , Sox-9 and BGLAP was analyzed by Flow cytometry.

2.9. Western blot

Total protein of ND-ASC, T1DM-ASC and CMTA was extracted. The protein sample was diluted after quantitative analysis, and denatured at 95 $^{\circ}\text{C}$ for 10 min. The sample was added to the SDS-PAGE colloidal pore and subjected to electrophoresis at 100 V for about 1.5 h (using Three-color prestain protein molecular marker (EC1019) as a reference, Shandong Sparkjade Biotechnology Co., Ltd.). After membrane transfer (200 mA, 60 min), 5% nonfat-dried milk was used to seal non-specific parts for 2 h at room temperature. After 4 rinses with TBST, membrane was incubated with primary antibodies overnight at 4 $^{\circ}\text{C}$. The primary antibodies used were: Anti-PPAR- γ (1:1000 dilution, abcam, ab178860), Anti-Sox-9 (1:1000 dilution, abcam, ab185230), Anti-ALP (1:1000 dilution, abcam, ab307726). Then after 4 rinses with TBST,

Table 2
Human genes primer sequences for qRT-PCR.

Genes	Primers (5'-3')
BGLAP-F	GCGCTACCTGTATCAATGG
BGLAP-R	TCAGCCAACCTCGTCACAGTC
PPAR- γ -F	GCTGGCCCTCCTTGATGAATA
PPAR- γ -R	TGCTTCAATGGGCTTCACA
Sox-9-F	TTCAGCAGCCAATAAGTG
Sox-9-R	GTGGAATGCTTTGAAGTTA

membrane was incubated with secondary antibodies (HRP-labeled Goat Anti-Rabbit IgG (H + L), 1:5000 dilution, Beyotime, A0208) for 2 h at room temperature. Finally, after 4 rinses with TBST and adding luminescent liquid (Sparkjade ECL super, ED0015, Shandong Sparkjade Biotechnology Co., Ltd.), the imaging system was used for exposure and image acquisition (Tanon5200).

2.10. Adipogenic, osteogenic, and chondrogenic differentiation

Adipogenic differentiation was conducted according to the instruction (Procell PD006, Wuhan, China). In details, ND-ASC, T1DM-ASC and CMTA were seeded at a density of 2.5×10^4 cells/cm² at 37 °C, 5% CO₂. When cells reached 100% confluent, the supernatant was discarded and the cells were incubated with adipogenic differentiation complete medium ADP1 for three days. Then, the medium was changed to complete medium ADP2, and the cells were incubated for 1 day. Then, complete medium ADP2 was replaced with complete medium ADP1 and incubated for another 3 days. After 4 times of alternating induction, complete medium ADP2 was used for another 3 days. Then adipogenic differentiation was assessed by Oil Red O staining of the fat droplets. The phase contrast image was photographed with an inverted fluorescence microscope (Olympus IX71, Tokyo, Japan).

Osteogenic differentiation was conducted according to the instruction (Procell PD007, Wuhan, China). In details, ND-ASC, T1DM-ASC and CMTA were seeded at a density of 2×10^4 cells/cm² at 37 °C, 5% CO₂. When cells reached 80% confluent, the medium was discarded and changed into osteogenic differentiation medium. The medium was subsequently changed every three days. After 21 days, osteogenic differentiation was assessed by Alizarin Red S staining. The phase contrast image was photographed with an inverted fluorescence microscope.

Chondrogenic differentiation was performed according to the instruction (Procell PD020, Wuhan, China). Briefly, ND-ASC and T1DM-ASC were collected in 500 μL of chondrogenic differentiation medium at a density of 2.5×10^5 cells, and then transferred into a 15 mL centrifuge tube and centrifuged at 150 g for 5 min. After centrifugation, the cell mass cannot be shaken or blown up. And the centrifuge tube cover was carefully loosed to facilitate gas exchange. The medium was subsequently changed every two days. After 28 days, the chondrospheres were fixed with neutral formaldehyde and processed for paraffin embedding. Chondrogenic differentiation was assessed by Alcian Blue staining. The phase contrast image was photographed with an upright fluorescence microscope (Olympus BX51, Tokyo, Japan).

2.11. Secretion activity of ND-ASC, T1DM-ASC and Cu-Mon-treated T1DM-ASC

Human Angiogenesis Panel 1 (10-plex) with V-Bottom Plate (Biolegend 740,698, California, USA) was used to analyze the proteins in the culture medium. Briefly, a selected panel of capture beads were mixed and incubated with 25 μL of culture medium for 2 h. After washing, a biotinylated detection antibody cocktail was added and incubated for 1 h. Then streptavidin-phycoerythrin (SA-PE) was then added and incubated for 30 min. Specific populations were segregated and PE fluorescence signal was quantified on a flow cytometer. The concentration of a particular analyte was determined using a standard curve.

2.12. ROS level of ND-ASC, T1DM-ASC and Cu-Mon-treated T1DM-ASC

Intracellular ROS level of ND-ASC, T1DM-ASC and Cu-MON-treated T1DM-ASC were studied. T1DM-ASC and ND-ASC was seeded in a 24-well plate with 1×10^5 cells/well, respectively. After incubation for 24 h, Cu-MON solutions were added to co-incubate with T1DM-ASC for 12, 24, 48, 72 h. The cells were collected for DCFH-DA staining, and then intracellular ROS were detected by flow cytometry (BD Accuri C6, New York, USA).

2.13. Cu-Mon enhance the paracrine effects of T1DM-ASC

The effect of Cu-MON on the interaction of T1DM-ASC with HUVEC, SMC, 3T3 and RAW264.7 was evaluated by macrophages polarization, migration, tube formation and cell proliferation assays.

First, co-culture supernatant of T1DM-ASC and Cu-MON (abbreviated as Cu-MON-CM) was obtained. Briefly, T1DM-ASC was seeded into a 24-well plate with a density of 1×10^5 cells per well and cultured for 24 h. Unless otherwise specified, the concentration of Cu-MON was 12.5 μg mL⁻¹ in the following experiments. Cu-MON was added and co-incubated with T1DM-ASC for 0.3, 1, 2, 4, 5 d. At corresponding time points, samples were centrifuged at 12,000 rpm for 15 min to remove cell debris and particles, and Cu-MON-CM was obtained after subsequent sterilization through a 0.22 μm filter, and stored at –80 °C until use.

Next, macrophage polarization induced by Cu-MON-CM was assessed, RAW264.7 were seeded into 24-well plates with a density of 1×10^5 cells per well. After incubation for 24 h, cells were treated with Cu-MON-CM for another two days. The morphology change of macrophages was observed under inverted microscope (BDS400, Chongqing, China). Besides, cells were collected for CD80 and CD206 staining, and then analyzed by flow cytometry. And the expression levels of IL-10, VEGF, TGF-β, IL-13, IL-4, IL-1β, TNF-α and IL-6 in RAW264.7 were detected by ELISA.

Afterwards, HUVEC, SMC, 3T3 were separately co-cultured with Cu-MON-CM and the cell migration, tube formation and proliferation were assessed. First, the cell migration was determined by a scratch test. HUVEC, SMC, 3T3 were separately seeded into a 24-well plate with a density of 5×10^4 cells per well and cultured for 24 h. Then the cells were vertically scratched with the head of 200 μL pipette tip. Floating cells were washed with PBS. Afterwards, the cells were treated with Cu-MON-CM for another 12 h. The photos of cells were taken under inverted microscope (BDS400, Chongqing, China) at 0 and 12 h. Image J software was used for data analysis.

$$\text{Migration (\%)} = (S0-ST)/S0 \times 100\%$$

where S0 and ST were the scratch area of cells at 0 h and 12 h, respectively.

The tube formation of cells was measured by precoating with BD Matrigel (Corning 356,234, New York, USA). 150 μL of Matrigel was added to a 24-well plate and placed in an incubator until the Matrigel layer solidified. HUVEC suspension was mixed with Cu-MON-CM, and 1 mL of pre-mixed cell suspension with a density of 6×10^4 cells/mL was added to Matrigel-coated wells, then incubated for another 6 h. The tubular formation was observed under inverted microscope, and the data analysis was performed by Image J software.

Cell proliferation was tested by CCK-8. HUVEC, SMC, 3T3 were separately seeded in a 96-well plate with a density of 5000 cells/well. After incubated for 24 h, cells were treated without or with Cu-MON-CM (half of culture media were replaced by Cu-MON-CM). At day 3, 10 μL of CCK-8 solution was added into each well and incubated for 1 h, and the OD value at 450 nm was measured using a microplate reader. Cell proliferation was evaluated according to a ratio of the OD value between experimental and control groups.

To real-time examination of T1DM-ASC paracrine effects on other cells, transwell assays were used to evaluate macrophage polarization, cell migration and tube formation. The effect of Cu-MON on the ability of T1DM-ASC to induce macrophage polarization. RAW264.7 were seeded in the lower chamber of the transwell insert with a density of 1×10^5 cells per well. After incubation for 24 h, T1DM-ASC, Cu-MON or Cu-MON treated T1DM-ASC (abbreviated CMTA) was added in the upper chamber of transwell and incubated for another 48 h. The morphology change of macrophages was observed under inverted microscope. Besides, cells were collected for CD80 and CD206 staining, and analyzed by flow cytometry. And the expression levels of IL-10, VEGF, TGF-β, IL-13,

IL-4, IL-1 β , TNF- α and IL-6 in RAW264.7 were detected by ELISA.

HUVEC (5×10^4 cells/well) were cultured in the lower chamber of transwell insert. After culture for 24 h, the cells were scratched. Then T1DM-ASC, Cu-MON or CMTA was added in the upper chamber and incubated for another 12 h. The photos of cells were taken under inverted microscope at 0 and 12 h. Image J software was used for data analysis.

$$\text{Migration (\%)} = (S0 - ST) / S0 \times 100\%$$

where S0 and ST were the scratch area of cells at 0 h and 12 h, respectively.

The tube formation ability of cells was measured. HUVEC suspension was cultured in the lower chamber (precoated with BD Matrigel) of transwell insert, and T1DM-ASC, Cu-MON or CMTA was severally added in the upper chamber. After co-culture for 6 h, the upper chamber was removed and the tube formation was observed under inverted microscope and the data analysis was performed by Image J software.

2.14. Protective effect of Cu-Mon on T1DM-ASC

In addition, the protective effect of Cu-MON on T1DM-ASC under adverse environment was verified. Briefly, T1DM-ASC was separately seeded in a 96-well plate with a density of 5000 cells/well. After incubated for 24 h, cells were treated without or with H₂O₂, PEI and UV exposure. After 24 h, 10 μ L of CCK-8 solution was added into each well and incubated for 1 h, and the OD value at 450 nm was measured using a microplate reader. Cell proliferation was evaluated according to a ratio of the OD value between experimental group and control group.

The mouse model of diabetic critical limb ischemia was prepared as reported in the literature [25]. After modeling, mice ($n = 3$) were randomly divided into three groups. After operation, ND-ASC (1×10^6 cells, abbreviated as Positive), T1DM-ASC (1.5×10^5 cells), Cu-MON-treated T1DM-ASC (1.5×10^5 cells after incubated with Cu-MON for 2 d, abbreviated as CMTA) were injected into the gastrocnemius. After 4, 24, 48, 72, 120, 168 h, the fluorescence intensity of hind limbs was monitored by small animal imaging instrument and the fluorescence intensity was analyzed by Image J.

2.15. Critical limb ischemia recovery

With reference [25,31] and more collateral vessels ligation, the mouse model of diabetic critical limb ischemia was prepared. After modeling, mice ($n = 6-8$) were randomly divided into eight groups. After operation, saline (abbreviated as Control), ND-ASC (1×10^6 cells, abbreviated as Positive), T1DM-ASC (1.5×10^5 cells), Cu-MON ($12.5 \mu\text{g mL}^{-1}$), Cu-MON-T1DM-ASC (1.5×10^5 cells after incubated with Cu-MON for 2 d, abbreviated as CMTA), conditioned medium (abbreviated as T1DM-ASC-CM), Cu-MON stimulated T1DM-ASC-conditioned medium (abbreviated as CMTA-CM) and ND-ASC-conditioned medium (abbreviated as ND-ASC-CM) were injected into the gastrocnemius in a scattered manner for 3 points. At day 0, 1, 7, 14, 21, 28, the necrosis of hind-limb was photographed and observed. During the experiment, the blood flow recovery of hind-limb was observed by full-field laser perfusion imager (moor FLPI-2, UK), and the perfusion ratio (ligation limb vs non-ischemic limb) was evaluated by moorFLPI-2 Review V5.0. At day 28, the stride length of recovering mice was measured. The leftpaws and rightpaws of the mice were dipped in red and blue nontoxic ink, respectively. The mice were confined to a running track made of paper (29.7-cm-long, 5-cm-wide). The stride length was determined by measuring the distance between two leftpaw prints and the area of the sole of the foot was quantified by Image J software. Besides, at day 28, 500 μ L of blood was collected through orbit blood collection, and serum was obtained by centrifugation. The levels of serum IL-6, TNF- α , IL-1 β , IL-10 were determined by ELISA. Besides, an appropriate amount of gastrocnemius muscle (the proportion of 100 μ L sample preparation

solution added per 10 mg tissue) was taken and homogenized at 4 $^{\circ}$ C. After centrifugation at 12,000 g for 5 min, the supernatant was taken to detect the levels of IL-6, TNF- α , IL-1 β , IFN- γ , MCP-1, GM-CSF, IP-10 and IL-10 (IFN- γ , MCP-1, GM-CSF and IP-10 mouse elisa kit were purchased from Shanghai Kexing Trading Co., Ltd, www.shfksc.com).

2.16. Histology and immunofluorescence

Mouse gastrocnemius following completion of the study at days 14 and 28 were bisected at the muscle centre. One-half was snap-frozen and stored at -80° C, while the other was fixed in 10 % formalin and processed for paraffin embedding. Sections of 6 μ m thickness were used and Hematoxylin and eosin (H & E) staining and Masson staining were performed. The gastrocnemius sections were stained by DHE (obtained from Beijing Solarbio Science & Technology Co. Ltd. Beijing, China) to evaluate ROS level in ischemic muscle. The stained slides were observed and images were taken under upright fluorescence microscope (Olympus BX51, Tokyo, Japan). The ROS expression was analyzed using Image J software.

For immunofluorescence, tissue sections were de-paraffinized, rehydrated. They were then blocked in 5% BSA for 40 min at room temperature and incubated with primary antibodies overnight at 4 $^{\circ}$ C in a humidified chamber. The primary antibodies used were: CD31 Polyclonal Antibody (1: 100, ThermoFisher PA5-32321), Alpha-Smooth Muscle Actin Monoclonal Antibody (1:250, ThermoFisher MA5-15805), iNOs Monoclonal Antibody (1:100, ThermoFisher 53-5920-82), CD206 Polyclonal Antibody (1:200, ThermoFisher PA5-101657), GS-IB4 (1:200, ThermoFisher I21411). Then they were incubated with secondary antibodies for 1 h prevented from light at room temperature. Sections were sealed with Mounting Medium, antifading (with DAPI) (Solarbio, S2110). Images were obtained at $\times 40$ magnification with an upright fluorescence microscope (Olympus BX51, Japan). Quantification was performed on Image J software by counting the positive cells/structures for a particular marker and dividing by the area of the tissue for normalization.

2.17. Statistical analysis

Data in vitro were presented as mean \pm standard deviation (Mean \pm SD), data in vivo were presented as mean \pm standard error (Mean \pm SEM). The Kolmogorov-Smirnov method was used to evaluate the normal distribution of data. One-way ANOVA was used to analyze data with only one variable. Two-way ANOVA was used to analyze the data with two variables. All analyses were performed using GraphPad Prism 8 software, and the significance was expressed as follows: * $P < 0.05$, ** $P < 0.01$, *** $P < 0.001$, **** $P < 0.0001$.

3. Results

3.1. Selection of optimal dose and time for Cu-Mon treated T1DM-ASC

In our previous work, copper-based metal-organic networks (Cu-MON) were generated by one-step reaction using anti-inflammatory and antioxidant baicalein as organic ligand and pro-angiogenic copper as metal ions. Cu-MON integrated the abilities of baicalein and copper ions to achieve redox homeostasis, inflammation inhibition, and angiogenesis promotion, and exhibited excellent capability in the treatment of critical limb ischemia with diabetes mellitus [25]. Here, Cu-MON was applied to improve the function of adipose-derived stem cells from type 1 diabetic donors (T1DM-ASC) and provide new options for the use of autologous stem cells in regenerative medicine.

First, cell viability of T1DM-ASC was assessed by CCK-8 after co-incubation with Cu-MON. As shown in [Supplementary Fig. 1A](#), the cell viability of T1DM-ASC decreased with increasing Cu-MON concentration, and there was no obvious cytotoxicity at concentrations lower than $12.5 \mu\text{g mL}^{-1}$. PI staining further confirmed the same results for up to 72

h (Supplementary Fig. 1B). An LDH release assay was also employed to evaluate the change in cell membrane permeability. As displayed in Supplementary Fig. 1C, no LDH release was observed after 72 h of incubation with $12.5 \mu\text{g mL}^{-1}$ of Cu-MON, suggesting that Cu-MON did not cause changes in cell membrane permeability. Therefore, $12.5 \mu\text{g mL}^{-1}$ of Cu-MON had no cytotoxicity on T1DM-ASC (unless otherwise specified, the concentration of Cu-MON was $12.5 \mu\text{g mL}^{-1}$ in the following experiments). Moreover, DCFH-DA was used to stain intracellular ROS. After co-incubation with Cu-MON, the intracellular ROS levels of T1DM-ASC decreased (Supplementary Fig. 1D), indicating that Cu-MON could reduce the level of oxidative stress induced by diabetes mellitus.

In the animal experiment, four doses (i.m. 2.5, 7.5, 12.5, and $17.5 \mu\text{g mL}^{-1}$) of Cu-MON were administered to select a safe dose. No significant differences in body weight were observed (Supplementary Fig. 1E). The serum levels of inflammatory cytokines were not increased (Supplementary Figs. 1F, G, H). In particular, $7.5 \mu\text{g}/\text{mouse}$ of Cu-MON decreased the levels of IL-6 and IL-1 β , which was beneficial for reducing the inflammatory response. There were no significant changes in the levels of anti-inflammatory cytokines (Supplementary Fig. 1I). Moreover, no obvious histological changes were found within major organs (Supplementary Fig. 1J), indicating that Cu-MON had good biocompatibility in vivo. Therefore, the dose of Cu-MON was chosen to be $7.5 \mu\text{g}/\text{mouse}$ for animal experiments unless otherwise specified.

In order to select the optimal incubation time for Cu-MON treated T1DM-ASC, the cell growth curve of T1DM-ASC was drawn. As displayed in Supplementary Fig. 2, during the first eleven days, the cell number continues to increase. The time required to double the number of cells was 2.326 ± 0.076 d. At this time, cells entered the logarithmic growth period, when the cell growth was most vigorous and the cell viability was relatively best. Therefore, we chose 2 d as the optimal time point for cell viability, and during the 2 d period, the cells grew relatively slowly, as the delay period, at which we randomly chose 0.3 d and 1 d as the co-incubation time points. In the time after 2 d, the cells entered the stable growth phase, during which we randomly selected 4 d and 5 d as co-incubation time points. The cytokine secretion of Cu-MON treated T1DM-ASC at 0.3 d, 1, 2, 4, and 5 d was evaluated. As shown in Supplementary Fig. 3, when incubated for 2 d, the secretion of angiogenesis related factors, VEGF, EGF, bEGF, NO, AngII, and IL-8 all increased. And the inflammatory cytokine IL-6 expression was decreased. Among them, VEGF, NO, AngII and IL-8 peaked at 2 d. Considering the cytokine secretion, Cu-MON treated T1DM-ASC for 2 d (CMTA) was selected as the experimental group. And, unless otherwise stated, the co-incubation time of Cu-MON was 2 d in the following experiments.

3.2. Endocytosis of T1DM-ASC on Cu-Mon

The endocytosis of T1DM-ASC on Cu-MON was studied. As shown in Supplementary Figs. 4, 5, 6, baicalein was labeled with Cy5, copper ion was labeled with Rhodamine B. The uptake of Cy5-Cu-MON by T1DM-ASC was higher than that of Cy5-BAI, suggesting that the formation of Cu-MON was conducive to the phagocytosis of BAI by T1DM-ASC. The phagocytic rate of Cu-MON-RB and Cy5-Cu-MON-RB in T1DM-ASC at 4 h were less than that of Cu-RB, which may be due to the fact that copper ions need more time to dissociate from Cu-MON, and its release is sustained and slow. As expected, at 48 h, phagocytosis of Cu-MON-RB and Cy5-Cu-MON-RB by T1DM-ASC was greater than 4 h, which helps avoid acute copper poisoning and continues to exert the effects of copper ions. These results indicate that Cu-MON can be endocytosed by cells to regulate its function.

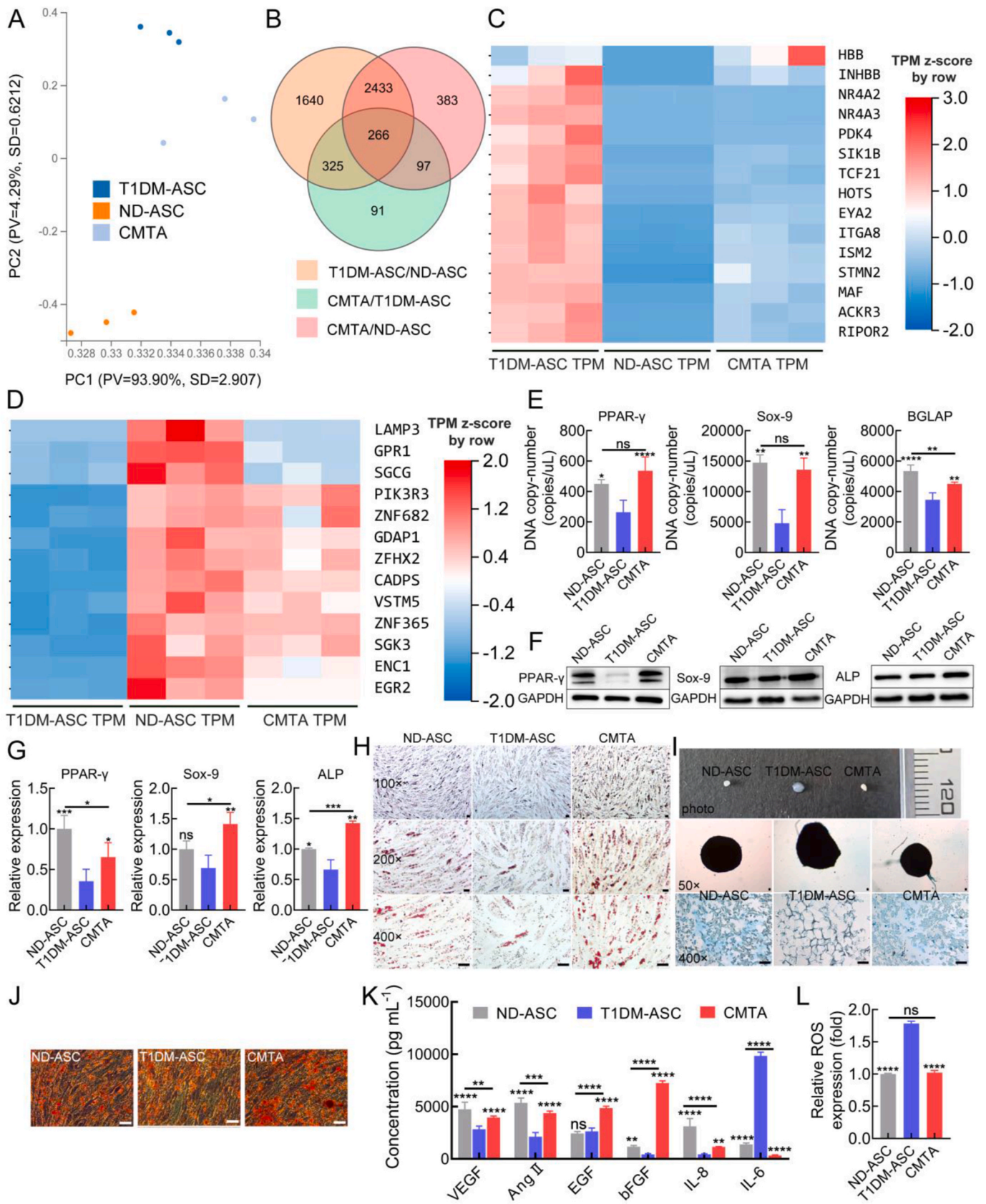
3.3. Stemness and transcriptional sequencing of T1DM-adipose stem cells after co-incubation with Cu-Mon

To elucidate the underlying defects of ASC during the disease

progression of type 1 diabetes mellitus (T1DM), we performed transcriptome sequencing analysis of adipose-derived stem cells from non-diabetic donors (ND-ASC) and adipose-derived stem cells from type 1 diabetic donors (T1DM-ASC). Furthermore, Cu-MON treated T1DM-ASC (abbreviated CMTA) was compared with ND-ASC and T1DM-ASC. Clear bands of 28 S and 18 S RNA were observed by RNA gel electrophoresis (Supplementary Fig. 7), suggesting that the RNA extraction was complete. The transcriptome profiles of T1DM-ASC greatly differed from that of the ND-ASC (Fig. 1A). Moreover, compared with ND-ASC and T1DM-ASC, CMTA was in the middle state of the two. There were 266 genes in the intersection of the three transcriptomes (Fig. 1B). Based on the clustering of the genes in $\log_2(T1DM-ASC/ND-ASC) \geq 7$, 15 genes were up-regulated in T1DM-ASC and down-regulated in CMTA compared to ND-ASC (Fig. 1C). Similarly, by clustering of the genes with $\log_2(T1DM-ASC/ND-ASC) \leq -4$, 13 genes were down-regulated in T1DM-ASC and up-regulated in CMTA compared to ND-ASC (Fig. 1D), suggesting that Cu-MON repaired the disease state in the cells of patients with diabetes. The KEGG network interaction was performed on the 266 genes of $|\log_2(T1DM-ASC/ND-ASC)| \geq 1$ (complete lists are presented in Dataset S1), and the results showed that these genes were closely related to Cytokine-cytokine receptor interaction, P13K-Akt signaling pathway, MAPK signaling pathway, Ras signaling pathway, Rap1 signaling pathway, Transcriptional misregulation in cancer, Pathways in cancer and Human papillomavirus infection (Supplementary Fig. 8A). In addition, PPI network construction was performed for these 266 genes based on GSEA. More than seven node connections were observed with CXCL10, OASL, IFIT2, HERC5, KIT, PCNA, ZBTB16 and H3-2 (Supplementary Fig. 8B), suggesting that Cu-MON regulate angiogenesis, the immune response, cell survival, antiviral activity, and anticancer activity to enhance functionality.

Furthermore, the effect of Cu-MON on the expression of ASC tri-directional differentiation genes was verified by qRT-PCR. As shown in Fig. 1E, Cu-MON enhanced the expression of PPAR- γ , Sox-9 and BGLAP in T1DM-ASC, indicating that Cu-MON enhanced the efficiency of adipogenesis, chondrogenic and osteogenic differentiation of T1DM-ASC, that is, enhanced the stemness of ASC. Flow cytometry results confirmed that compared with ND-ASC, PPAR- γ , Sox-9 and BGLAP expression were decreased in T1DM-ASC, and then increased after Cu-MON treatment (Supplementary Fig. 9). Intracellular proteins were extracted and the expression of response proteins was verified by Western blot. Considering that BGLAP is expressed in the late osteogenesis, therefore, ALP expressed in the early osteogenesis was chosen to evaluate osteogenic differentiation. As expected, compared with ND-ASC, PPAR- γ , Sox-9 and ALP expression were decreased in T1DM-ASC, and then increased in CMTA (Fig. 1F and G). Furthermore, the adipogenic, chondrogenic and osteogenic differentiation capacity of ND-ASC, T1DM-ASC and CMTA were assessed by staining. As shown by Oil Red O staining, smaller and fewer adipose droplets were generated from T1DM-ASC of adipogenic differentiation compared with ND-ASC group, and the number of adipose droplets increased in CMTA group (Fig. 1H). The chondrospheres induced by T1DM-ASC appeared to be larger than those induced by ND-ASC and CMTA (Fig. 1I). In fact, the internal structure of T1DM-ASC was loose and destroyed after Alcian Blue staining. The internal structure of chondrospheres in CMTA group was similar to that of ND-ASC. Similar to adipogenic differentiation, CMTA showed strong osteogenic differentiation ability as confirmed by Alizarin Red S staining (Fig. 1J). These results indicated that T1DM-ASC have impaired adipogenic, chondrogenic and osteogenic differentiation potential of ND-ASC group, while Cu-MON pretreatment restored the function of T1DM-ASC.

Protein expression related to angiogenesis and immune regulation was examined. As displayed in Fig. 1K, compared with ND-ASC, the expression levels of angiogenesis-related cytokines (VEGF, AngII, FGF, IL-8, etc.) in T1DM-ASC were significantly decreased, while the expression levels the inflammatory cytokine IL-6 were significantly increased. The co-incubation of T1DM-ASC with Cu-MON significantly



(caption on next page)

Fig. 1. Differences in transcriptome, tri-directional differentiation ability and secretome between ND-ASC, T1DM-ASC and CMTA. (A) PCA plot illustrating the variances of ND-ASC, T1DM-ASC and CMTA. (B) VENN diagram of T1DM-ASC/ND-ASC, CMTA/T1DM-ASC, CMTA/ND-ASC. (C) Heatmap representing expression of z-score of the 15 differentially expressed genes from blue (low expression) to red (high expression). $Q_{\text{value}} < 0.05$ and $|\log_2(\text{T1DM-ASC/ND-ASC})| \geq 7$. (D) Heatmap representing expression of z-score of the 13 differential genes from blue (low expression) to red (high expression). $Q_{\text{value}} < 0.05$ and $\log_2(\text{T1DM-ASC/ND-ASC}) \leq -4$. (E) Gene expression of PPAR- γ , Sox-9 and BGLAP in ND-ASC, T1DM-ASC and CMTA (after treatment with Cu-MON for 2 d). (F) Protein expression of PPAR- γ , Sox-9 and ALP in ND-ASC, T1DM-ASC and CMTA. (G) The relative expression of PPAR- γ , Sox-9 and ALP analyzed by Image J software. (H) The morphology of adipogenic differentiation by Oil Red O staining ($100\times$, $200\times$ and $400\times$ magnification). (I) The morphology of chondrogenic differentiation by Alcian Blue staining ($400\times$ magnification). (J) The bottom image is a direct view of the cartilaginous sphere. The middle photograph was taken under an optical microscope ($50\times$ magnification). The below image shows the morphology of osteogenic differentiation by Alizarin Red S staining ($400\times$ magnification). (K) Levels of cytokines secreted by CMTA, T1DM-ASC and ND-ASC. (L) Flow cytometry analysis of relative expression levels of intracellular ROS in ND-ASC, T1DM-ASC and CMTA (treated with Cu-MON for 3 d). The graph on the right is the histogram of the bar chart. The data are presented as the mean \pm SD ($n = 3$, Compared to T1DM-ASC, same below unless otherwise labeled, * $P < 0.05$, ** $P < 0.01$, *** $P < 0.001$ and **** $P < 0.0001$).

increased the expression of VEGF, AngII, EGF, FGF, IL-8 and NO, and significantly decreased the expression of IL-6 (Fig. 1L, Supplementary Fig. 3). These findings indicate that Cu-MON attenuated the inflammatory response and activated the expression of angiogenic factors, which is consistent with the results in Supplementary Fig. 8. Moreover, Cu-MON decreased the oxidative stress level of T1DM-ASC (Fig. 1L).

Next, to better understand the mechanism by which Cu-MON enhanced the stemness and transcriptomic recovery of T1DM-ASC, we compared CMTA with T1DM-ASC for detailed analysis. Transcriptomic analysis identified 779 differentially transcribed genes in CMTA and T1DM-ASC, including 353 significantly up-regulated genes and 426 significantly down-regulated genes (Fig. 2A, Dataset S2). Among the top 13 significantly differentially expressed genes, four genes (LAMP3, CXCL10, CXCL11 and RSAD2) were also expressed in HUVEC [32,33], two genes (MT1X and RSAD2) were also expressed in Myoblast, one gene (MT1X) was also expressed in Myofibroblast and Vascular Smooth Muscle (Fig. 2B). These findings possibly infer common roles for these cell types. These highly expressed genes had a positive influence on cell functions, such as regulating chronic inflammation [34,35], resisting oxidative stress [36,37], promoting endothelial cell proliferation [38], participating in the recruitment of fibroblasts and endothelial cells [39], and promoting angiogenesis [40,41]. GO and KEGG analyses of the top differentially expressed genes highlighted the enrichment of multiple processes linked to Cytokine-cytokine receptor interaction (Fig. 2C and D). Based on gene set enrichment analysis (GSEA), a protein-protein interaction (PPI) network was constructed using mRNAs associated with paracrine pathways. Twelve nodes with high connectivity with CXCL10 were observed, suggesting that Cu-MON promoted monocyte chemotaxis, endothelial cell migration and neovascularization (Fig. 2E). Moreover, among all the altered genes, the up-regulated genes were significantly enriched with Viral protein interaction with cytokine and cytokine receptor, Cytokine-cytokine receptor interaction, Toll-like receptor signaling pathway, TNF signaling pathway, Longevity regulating pathway - worm (Fig. 2F), suggesting that Cu-MON treatment was mainly involved in the paracrine pathway of ASC. The down-regulated genes were significantly enriched with MAPK signaling pathway, Rap1 signaling pathway, PI3K-Akt signaling pathway, TGF-beta signaling pathway, Growth hormone synthesis, secretion and action, cGMP-PKG signaling pathway, Parathyroid hormone synthesis, secretion and action (Fig. 2G), suggesting that Cu-MON regulated the growth, differentiation and stress and inflammatory responses of ASC. Specifically, IL-6 and IL-1 β expression levels of T1DM-ASC were significantly decreased in the presence of Cu-MON (Supplementary Fig. 10), indicating that Cu-MON treatment induced transcriptional regulation were tightly associated with a reduction in inflammation. Furthermore, the expression levels of many cancer-related genes (34 out of 80 genes) was also decreased after Cu-MON treatment (Fig. 2G), suggesting that Cu-MON could reduce the tumorigenicity of stem cells. Collectively, these findings indicated that the treatment of T1DM-ASC with Cu-MON can enhance multiple repair processes, including immune regulation, cell migration, and angiogenesis, to promote ischemic repair.

In summary, the transcriptomic and protein expression data supported a rescued pathological phenotype, possibly through the

activation of T1DM-ASC activity and enhancement of T1DM-ASC stemness. These effects promote paracrine effects and cell-cell interactions and induce pro-angiogenic protein expression, thus leading to a partial recovery of the regulated transcriptome after induction.

3.4. *In vitro* therapeutic potential of T1DM-ASC after co-incubation with Cu-Mon

MSC have been reported to extensively regulate the activation and function of various immune cells, including macrophages [42,43]. Therefore, considering that ASC is a type of MSC, the effects of T1DM-ASC and CMTA on macrophage function were investigated. First, conditioned medium from T1DM-ASC (abbreviated as CM) and conditioned medium from CMTA (abbreviated as Cu-MON-CM) were collected at different time points to investigate their effects on macrophage polarization. A schematic diagram is shown in Fig. 3A. The morphology of RAW264.7 cells shifted from a round shape to a spindly shape after incubation with Cu-MON-CM (Fig. 3B). M2 macrophages were quantified using CD206 immunofluorescence staining. Cu-MON-CM was found to be a stimulus of M2 macrophage polarization, which peaked using Cu-MON-CM after two days of incubation (Fig. 3C). Thereafter, secreted cytokines from polarized macrophages were also assessed. As expected, macrophages treated with Cu-MON-CM secreted more anti-inflammatory cytokines and angiogenic factors, such as IL-10, IL-13, IL-4, VEGF and TGF- β , and less pro-inflammatory cytokines, such as IL-1 β , TNF- α and IL-6 (Fig. 3D, Supplementary Fig. 11).

The impact of Cu-MON-CM on HUVEC migration capacity was further investigated using a scratch assay. A schematic diagram is shown in Fig. 3A. Cu-MON-CM from 2 days of incubation showed the greatest potential in promoting migration (Fig. 3E and F), whereas Cu-MON-CM from a shorter incubation time (e.g., 12 h) showed no difference in promoting migration compared to the control group (Supplementary Figs. 12A and B). A similar trend was also observed in the tube formation assay (Fig. 3G and H), where Cu-MON-CM from 2 days of incubation produced the most nodes, longest branching length and most capillary-like networks. Application of such scratch assays to SMC and 3T3 cell lines also yielded similar results (Supplementary Figs. 12C–F). Furthermore, the effect of Cu-MON-CM on the viability of RAW264.7, SMC, 3T3 and HUVEC were assessed. As shown in Supplementary Fig. 13, Cu-MON-CM from any time points did not cause a decrease in cell viability; instead, Cu-MON-CM from two days of incubation promoted the proliferation of SMC and 3T3. These results suggested that conditioned medium from Cu-MON and T1DM-ASC coculture, especially those incubated for two days, effectively promoted M2 macrophage polarization, and the migration and tube formation of HUVEC, thus, it possesses the potential in inflammation alleviation, angiogenesis and tissue repair. This was because the cytokine-cytokine receptor interaction was promoted after Cu-MON incubation, and some genes significantly altered by T1DM-ASC were also expressed in endothelial cells, fibroblasts and smooth muscle cells (Fig. 2B), suggesting the combined effects of these cells and the cascade effect on angiogenic repair.

Successful tissue repair is a well-orchestrated process that involves multiple cell-cell interactions [44,45]. To better simulate the *in vivo*

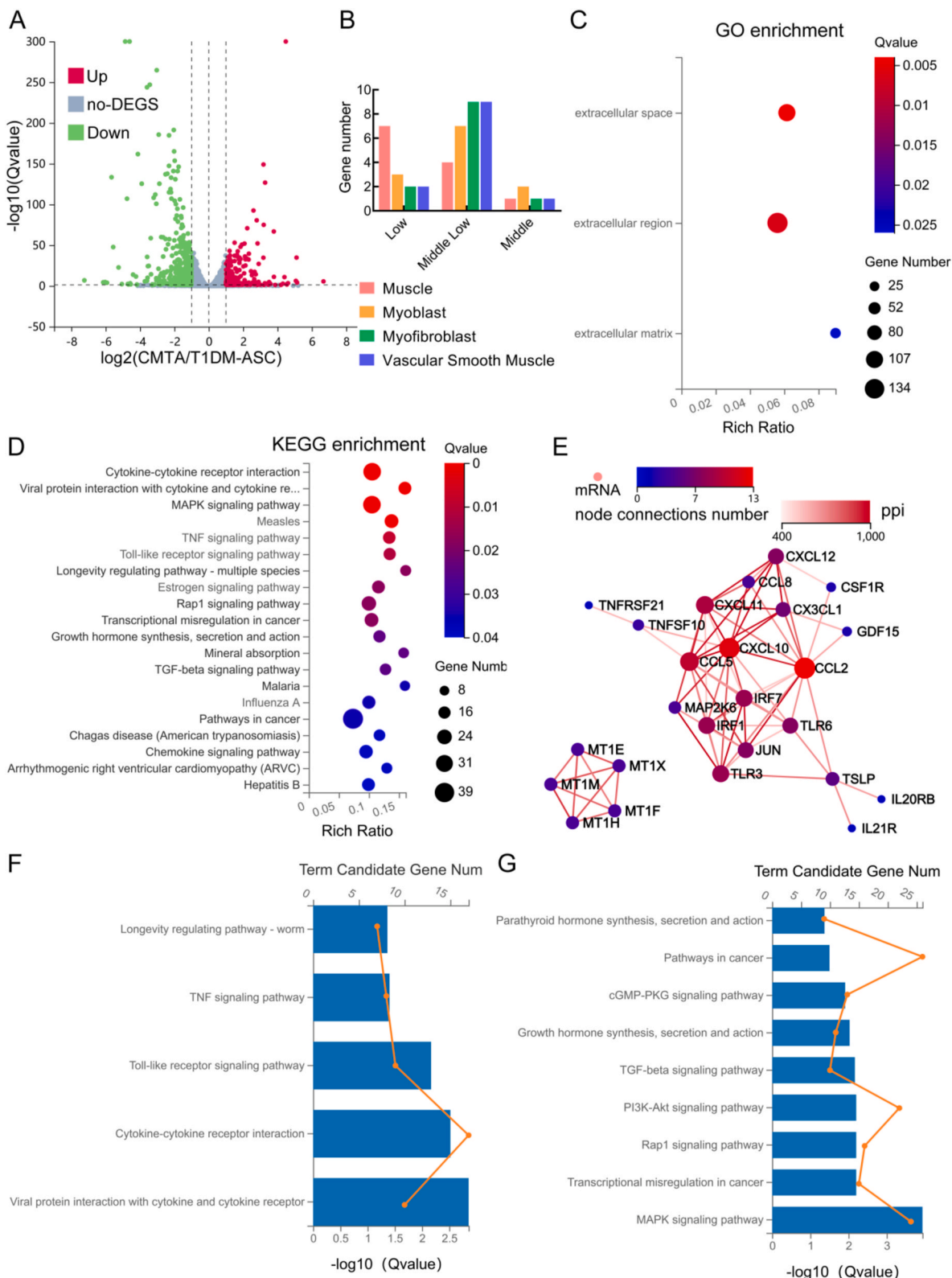


Fig. 2. Transcript Sequencing differences and performance differences between T1DM-ASC and CMTA. (A) Volcano plot showing that 779 genes are differentially regulated between CMTA and T1DM-ASC. The $\log_2(\text{Fold-Change})$ was estimated by DESeq2. $Qvalue < 0.05$ and $|\log_2(\text{fold change})| \geq 1$. (B) Gene number and level of the top 13 differentially expressed genes expressed in Muscle, Myoblast, Myofibroblast and Vascular Smooth Muscle. (C) GO analysis of differentially modulated genes classified by their biological functions and arranged according to their statistical significance. (D) KEGG analysis of differentially modulated genes classified by their biological functions and arranged according to their statistical significance. (E) Protein-protein interaction networks based upon the up-regulated by GSEA. Kyoto Encyclopedia of Genes and Genomes (KEGG) analysis of up-regulated gene (F) and down-regulated gene (G) classified by their biological functions and arranged according to their statistical significance. The data are presented as the mean \pm SD ($n = 3$, * $P < 0.05$, ** $P < 0.01$, *** $P < 0.001$ and **** $P < 0.0001$).

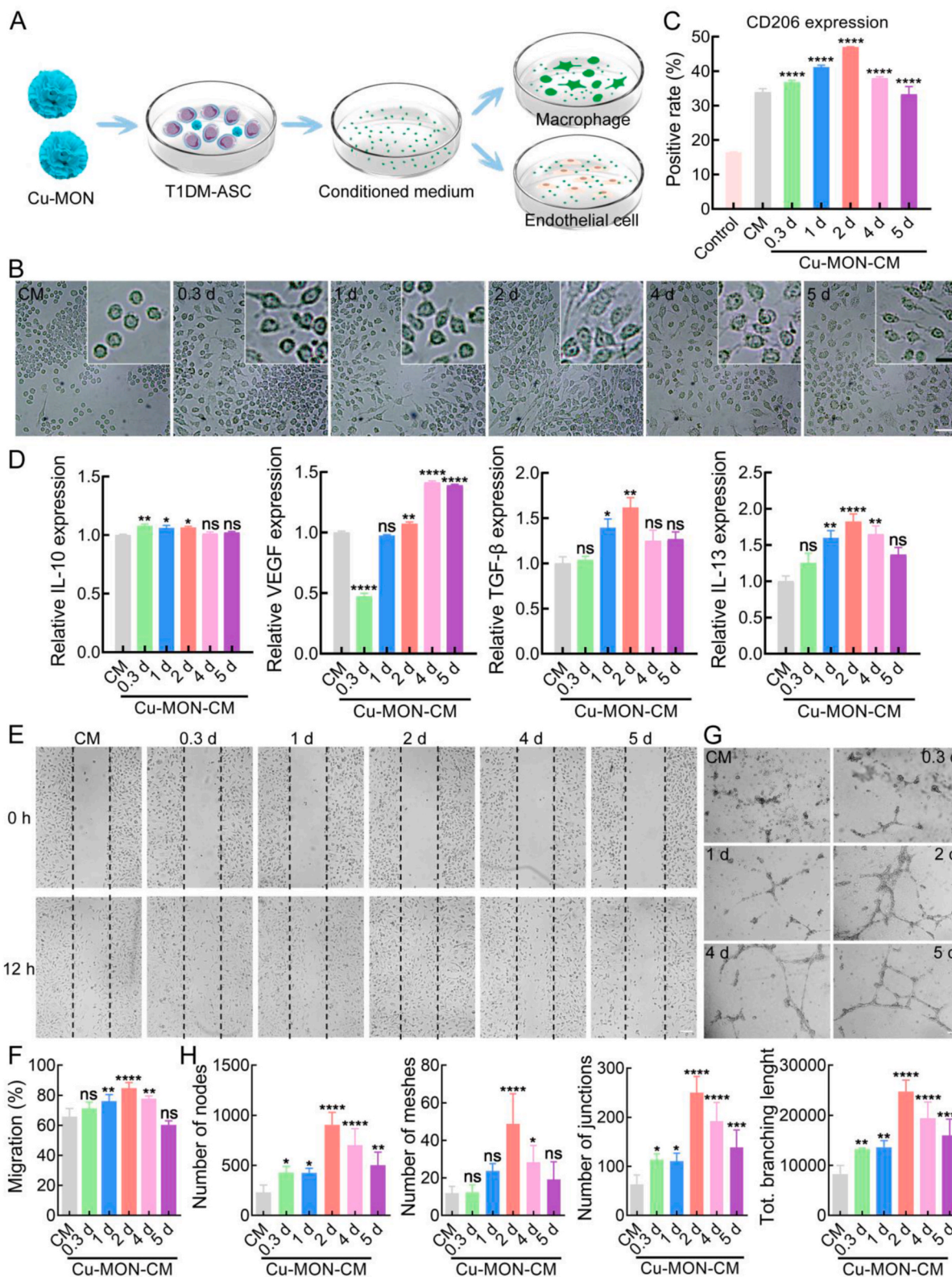


Fig. 3. Cu-MON indirectly promoted the effect of T1DM-ASC on macrophage polarization, HUVEC migration and tube formation through conditioned medium. (A) Schematic diagram of the experimental process investigating the effect of conditioned medium. (B) Representative optical images of RAW264.7 cells treated with CM and Cu-MON-CM for 2 d, Bar = 50 μm. The inset picture was 3 × magnification of figure B, Bar = 20 μm. (C) Flow cytometry analysis of CD206 expression after treating RAW264.7 cells with CM and Cu-MON-CM for 2 d. (D) The levels of IL-10, VEGF, TGF-β, and IL-13 in the supernatants. (E) Representative images of HUVEC migration after treatment with CM and Cu-MON-CM for 12 h, Bar = 50 μm. (F) The migration rate of HUVEC analyzed by Image J software. (G) Representative images of HUVEC tubular formation after treatment with CM and Cu-MON-CM for 6 h (Bar = 50 μm), and (H) their quantitative analysis using Image J software. The data are presented as the mean ± SD (n = 3, *P < 0.05, **P < 0.01, ***P < 0.001 and ****P < 0.0001).

environment, Transwell chambers were used to investigate the effects of CMTA on RAW264.7 and HUVEC (Fig. 4A). First, the effects of Cu-MON, T1DM-ASC and CMTA on macrophage polarization were evaluated. The morphology of RAW264.7 changed after coculture with Cu-MON, T1DM-ASC and CMTA (Fig. 4B). CMTA had the highest ratio of M2 to M1 as compared with T1DM-ASC, Cu-MON and Control (Fig. 4C). Furthermore, CMTA significantly increased the expression of M2 macrophage-related factors, such as IL-10, VEGF, IL-13 and IL-4, and down-regulated the expression of M1 macrophage-related factor IL-1 β (Fig. 4D). Interestingly, the expression levels of TGF- β , IL-6 and TNF- α did not change significantly, which was different from the previous Cu-MON-CM experiment (Fig. 3D, Supplementary Fig. 11). A more complex interaction via cytokines when cells were cocultured is a possible explanation for these findings, and these interactions may act through synthesis and secretion, receptor expression and biological effects [46]. In turn, they form a complex network of interactions and act not just through single-cell cytokine changes [46].

In the scratch assay, CMTA significantly promoted HUVEC migration, followed by Cu-MON and T1DM-ASC (Fig. 4E and F). Similar results were also observed in SMC and 3T3 (Supplementary Fig. 14). In the tube formation assay, CMTA resulted in more nodes, meshes, and capillary-like structures than Control and was superior to T1DM-ASC, Cu-MON (Fig. 4G and H). These results suggested that CMTA treatment enhanced M2 macrophage polarization, as well as migration and tube formation of HUVEC in vitro and thereby had great potential in tissue repair.

In addition, the protective effect of materials on T1DM-ASC was crucial due to external stimulation-induced damage during cell culture and elevated ROS levels at ischemic sites after cell transplantation. To evaluate the protective effect of Cu-MON on T1DM-ASC, high concentrations of hydrogen peroxide, PEI and UV exposure were used to simulate damage. Ultra-high concentrations of H₂O₂ (>125 μ M) caused cell death, as shown in Supplementary Fig. 15A. At higher concentrations of H₂O₂ (12.5–100 μ M), the cell viability of T1DM-ASC was significantly higher in the presence of Cu-MON. CMTA showed a trend of cell growth at 62.5 μ M of H₂O₂. Exposure of cells to PEI or UV light irradiation resulted in cytotoxicity [47]. As shown in Supplementary Fig. 15B and C, Cu-MON treatment rescued the cell viability of T1DM-ASC with increasing concentrations of PEI or prolonged UV exposure. The above results indicated that Cu-MON improved T1DM-ASC resistance and enhanced the viability of T1DM-ASC in a pathological microenvironment.

3.5. Treatment of critical limb ischemia in diabetic mice

The survival of T1DM-ASC, CMTA and ND-ASC in vivo was studied by establishing a limb ischemia model. According to previous reports, 10⁶ hMSCs were deemed as the minimum number to convey therapeutic effect in mice CLI treatments [48], therefore, 10⁶ of ND-ASC was chosen as a positive control. The dose of CMTA was set at 1.5 \times 10⁵, which was calculated according to our previous animal experiments and the optimal concentration of Cu-MON-treated T1DM-ASC. Specifically, in our previous animal experiments, the dose of Cu-MON was set at 7.5 μ g. When treating T1DM-ASC with Cu-MON, 12.5 μ g mL⁻¹ of Cu-MON is a safe and effective dose. According to cytokine secretion experiment, cytokine secretion of 2 d incubation was the highest, suggesting that the cells treated with Cu-MON for 2 d had an optimal quality. Therefore, after treating 1 \times 10⁵ of T1DM-ASC with 12.5 μ g of Cu-MON for 2 d, the cells were collected and the cell count was 2.5 \times 10⁵ due to proliferation. In other words, when Cu-MON was administered at 7.5 μ g, the number of T1DM-ASC cells should be set at 1.5 \times 10⁵. In summary, 1.5 \times 10⁵ of T1DM-ASC, 1.5 \times 10⁵ of CMTA, 1 \times 10⁶ of ND-ASC were stained with Did and injected to gastrocnemius. As shown in Fig. 5A and B, the fluorescence decreased in all groups over time. The fluorescence of the CMTA group was stronger than the T1DM-ASC and ND-ASC groups at all time points. The reason was that pretreatment with Cu-MON enhanced

the resistance of T1DM-ASC to adverse environments, which was consistent with the results in Supplementary Fig. 15.

Diabetes is a high risk factor for critical limb ischemia, which is also cured by ASC [49,50]. Therefore, a mouse model of diabetic critical limb ischemia was established to further investigate the angiogenic effect of Cu-MON-treated T1DM-ASC. ND-ASC (1 \times 10⁶ cells) was set as the positive group. Diabetic mice successfully induced by STZ (160 mg kg⁻¹) were subjected to femoral artery ligation and excision (Supplementary Fig. 16A). Blood flow recovery was assessed with a perfusion imager (FLPI-2, Moor Instrument, UK), and the region of interest (ROI) was the calf and foot in the supine position. At day 1, a sudden decrease in blood perfusion was observed in all mice, indicating the successful establishment of diabetic critical limb ischemia. At day 4, the blood flow recovery of Positive group was better than that of T1DM-ASC group and the CMTA group, possibly due to the dose-dependent effect of cell therapy within 1 \times 10⁶ cell number [51–53]. Interestingly, at day 7, the blood flow recovery of CMTA group was better than that of Positive group, as the perfusion ratio was highest in the CMTA group compared with all other groups. Notably, this superior therapeutic effect of T1DM-ASC pretreated with Cu-MON was achieved using only 15% of the untreated cell dose. These results suggested that Cu-MON pretreatment could enhance the therapeutic effect of T1DM-ASC and significantly reduce the effective dose required for cell therapy (Supplementary Fig. 16 B, C). At day 14, the blood perfusion of CMTA group basically returned to normal and the limbs of the mice were intact (Supplementary Fig. 16C, D). The limb ischemia of mice in Control group was the most severe, with blackened toes and curled footpads. In the remaining groups, only a few mice had black nails, open paws, and ruddy footpads. From the results of H&E staining, the pathological conditions of ischemic muscles in each treatment group also showed the same trend. Myofiber rupture, atrophy, rhabdomyolysis accompanied by massive inflammatory cell infiltration were observed in Control group. T1DM-ASC treatment partially improved muscle fiber atrophy, but myofiber rupture and inflammatory cell infiltration were still evident. In Positive group, myofiber ischemia was alleviated, as indicated by narrower inter-myofiber spaces and less inflammatory cell infiltration. The muscles in CMTA group were arranged regularly and tightly, similar to those in healthy muscles. In addition, there was no difference in the histological morphology of the heart, liver, spleen, kidney, intestines and testis in T1DM-ASC, Positive, CMTA groups compared to Control group (Supplementary Fig. 17). Notably, pulmonary inflammation was observed in the T1DM-ASC group of mice, but not in CMTA group. It may be because Cu-MON promoted the homing of T1DM-ASC, which was consistent with the result that Cu-MON increased the expression of chemokine CXCL10 in T1DM-ASC (Supplementary Fig. 8B). Moreover, CMTA significantly decreased the levels of serum IL-6 and TNF- α compared with those in Control group (Supplementary Fig. 18). Altogether, these results suggested that CMTA had a superior therapeutic effect on diabetic hindlimb ischemia in mice.

In our previous animal experiment, the femoral artery was ligated and all collateral vessels remained intact. To further test the pro-angiogenic ability, the femoral artery was ligated and all collateral vessels were cauterized and excised (Fig. 5C). This led to more severe ischemic manifestations, such as foot necrosis, gangrene and even limb loss. From the pictures of mice hind-limbs, compared with Control group, the T1DM-ASC, CMTA, and Positive group demonstrated blood flow recovery effects (Fig. 5D). At day 28, the toes of mice in T1DM-ASC, CMTA and Positive group were blackened, whereas mice in Control group developed toe gangrene. Moreover, CMTA and Positive group had improved foot curled-up status. Laser Doppler results at day 7 showed that the order of the degree of blood flow recovery was Positive group, CMTA group and then T1DM-ASC group (Fig. 6A and B). At day 14, the CMTA group had better blood flow recovery than the Positive group, which was due to the enhanced resistance of T1DM-ASC in the pathological microenvironment after Cu-MON treatment. At day 21, CMTA achieved a similar therapeutic effect to that of Positive group, and this

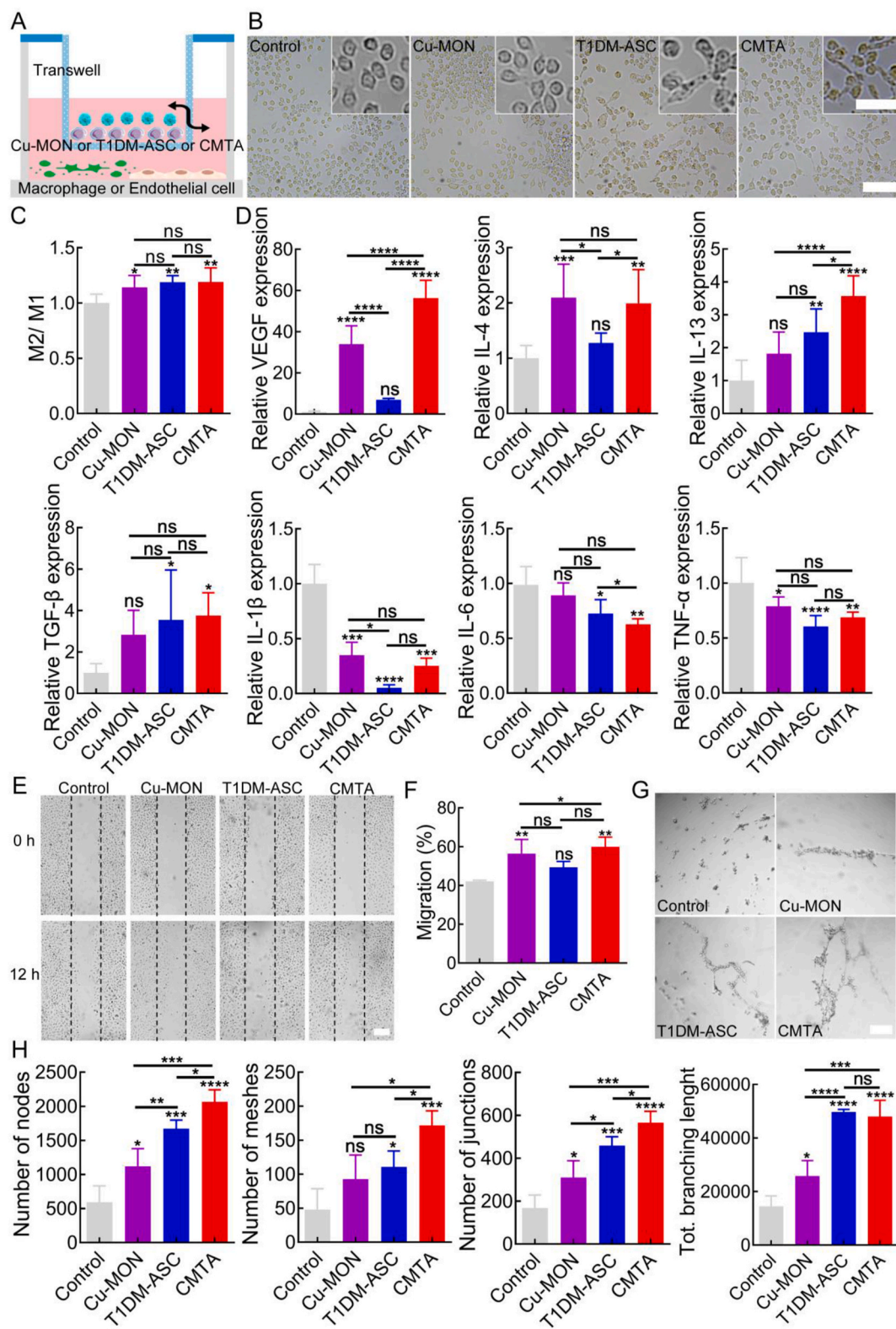


Fig. 4. Cu-MON directly promoted the effect of T1DM-ASC on macrophage polarization, HUVEC migration and tube formation through Transwell co-incubation. (A) Schematic diagram of the experimental process investigating the interaction of T1DM-ASC with macrophages and HUVEC using the Transwell compartment. (B) Representative optical images of RAW264.7 treated with Cu-MON, T1DM-ASC and CMTA, Bar = 50 μ m. The inset picture was 3 \times magnification of figure B, Bar = 20 μ m. (C) Flow cytometry analysis of CD206 expression after treating RAW264.7 with Cu-MON, T1DM-ASC and CMTA for 2 d. (D) The levels of IL-10, VEGF, TGF- β , IL-13, IL-4, IL-1 β , TNF- α and IL-6 in the supernatants. (E) Representative images of HUVEC migration after treatment with Cu-MON, T1DM-ASC and CMTA for 12 h, Bar = 50 μ m. (F) The migration rate of HUVEC analyzed by Image J software. (G) Representative images of HUVEC tubular formation after treatment with Cu-MON, T1DM-ASC and CMTA for 6 h (Bar = 50 μ m), and (H) their quantitative analysis using Image J software. The data are presented as the mean \pm SD (n = 3, *P < 0.05, **P < 0.01, ***P < 0.001 and ****P < 0.0001).

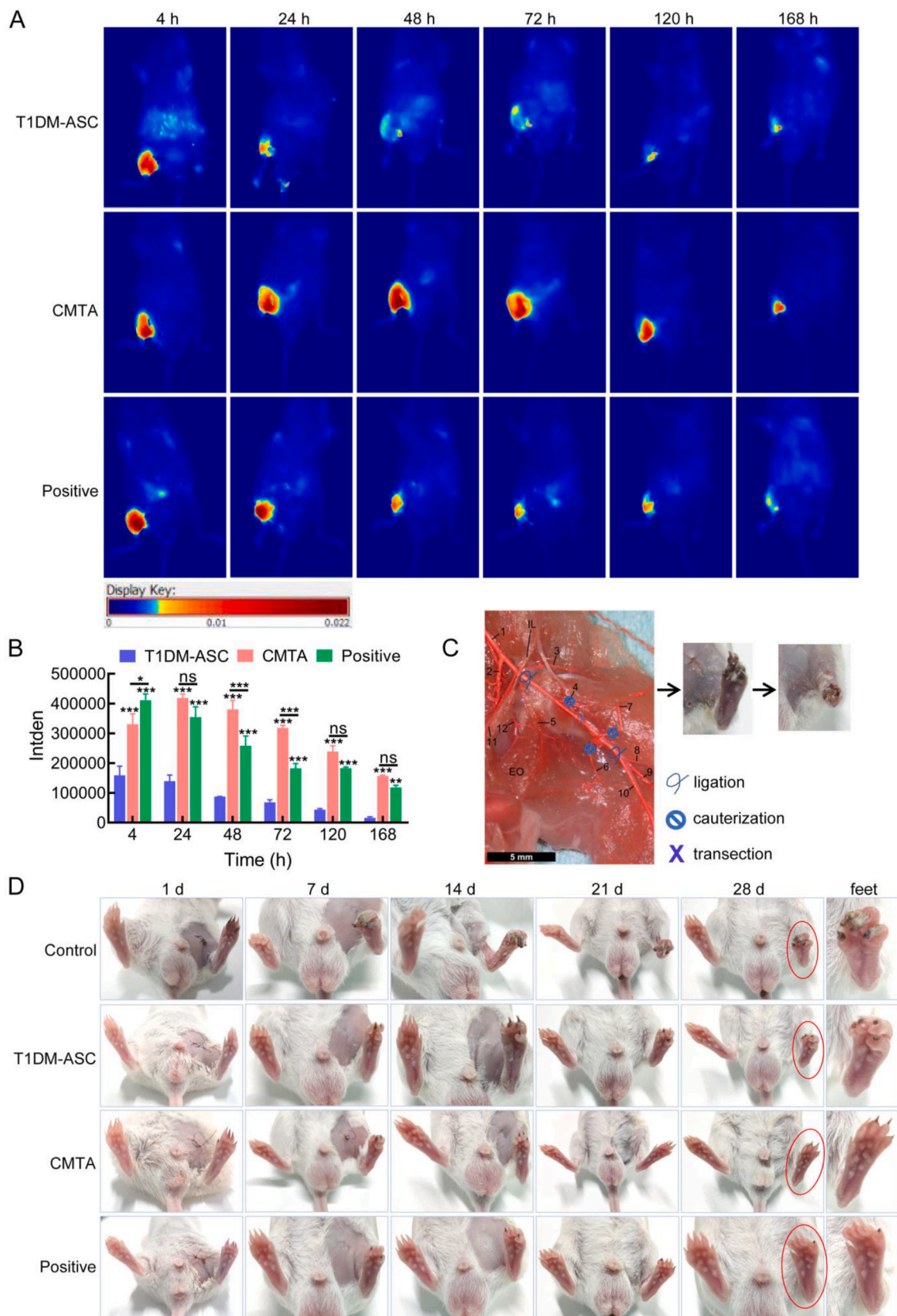


Fig. 5. Cu-MON treatment enhanced cell survival and reduced limb necrosis. (A) Fluorescence distribution in limbs at different time points. (B) Quantification of fluorescence intensity by Image J. (C) Schematic diagram of the operation. Picture from the literature [54]. (D) Representative photos of ischemic limbs at days 1, 7, 14, 21, 28 d after surgery. The data are presented as the mean \pm SEM ($n = 3-6$, * $P < 0.05$, ** $P < 0.01$, *** $P < 0.001$ and **** $P < 0.0001$).

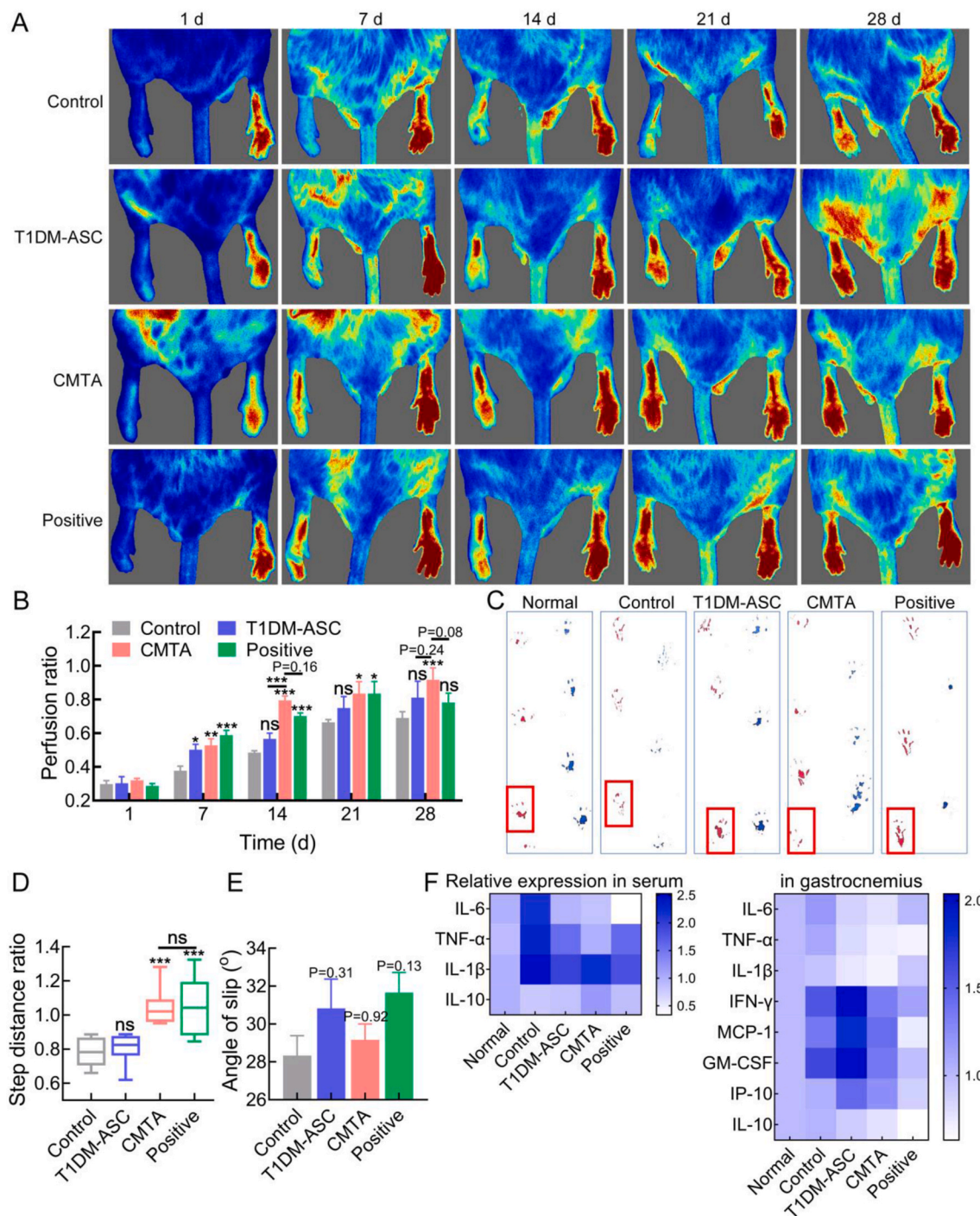


Fig. 6. Therapeutic effect of CMTA on critical limb ischemia in diabetic mice. (A) Representative Laser Doppler imaging of ischemia limb at days 1, 7, 14, 21, 28 after surgery. (B) The perfusion ratio of ischemia limb analyzed by moorFLPI-2 Review V5.0 attached to Laser Doppler imaging. (C) Representative image of footprint at day 28. Red ink represents the left foot, and blue ink represents the right foot. (D) Quantification of step distance. (E) Quantification of falling height. (F) Levels of IL-6, TNF- α , IL-1 β , IL-10 in serum and levels of IL-6, TNF- α , IL-1 β , IFN- γ , MCP-1, GM-CSF, IP-10 and IL-10 in gastrocnemius. The data are presented as the mean \pm SEM ($n = 3-6$, * $P < 0.05$, ** $P < 0.01$, *** $P < 0.001$ and **** $P < 0.0001$).

effect was better than that of T1DM-ASC group. Notably, the number of cells used in CMTA group was 1.5×10^5 , which was only 15% of that used in Positive group, suggesting that Cu-MON enhanced the function of T1DM-ASC. In addition, critical limb ischemia often leads to intermittent claudication and decreased walking ability [55], so the improvement of motor function and the recovery of muscle strength in mice with critical limb ischemia were evaluated. Footprinting experiments showed that mice in Control group had obvious lameness. The footprints of mice in T1DM-ASC were relatively complete, but the step

distance of the left foot was still less than that of the right foot, and the footprints of Positive group and CMTA group were intact and the step distance were similar to the right foot (Fig. 6C). As shown in Fig. 6D and E, there was a significant difference in step distance and slip angle between the CMTA and Control groups, indicating that CMTA significantly promoted the hindlimb motor function of the mice. Moreover, compared with the those in Control group, the serum levels of IL-6, TNF- α , and IL-1 β in CMTA group were decreased, and the serum levels of IL-10 in CMTA group were increased (Fig. 6F, Supplementary Fig. 19). And IL-6,

TNF- α , and IL-1 β expression were also decreased in ischemic muscle. Moreover, decreased expression of IFN- γ , MCP-1, GM-CSF and IP-10 indicated that CMTA treatment inhibited inflammatory response of diabetic mice.

The results of H&E staining showed that the myofibers of gastrocnemius muscle in Control group were atrophied with sharply blurred borders and extensive inflammatory cell infiltration (Fig. 7A). In contrast, in T1DM-ASC, CMTA, and Positive group, the morphology of myofibers was significantly improved, and the nuclei were scattered and regular along the edges. Furthermore, the inflammatory cell infiltration of CMTA group was improved as compared to the Positive group. At day 28, compared with that in Control, T1DM-ASC and Positive groups, the

muscle structure of mice in CMTA group was complete, and no obvious inflammatory cells were observed. These findings suggest that CMTA treatment promoted the repair of ischemic muscle. The results of Masson staining showed that both the Control and T1DM-ASC groups had more blue collagen fibers and disordered muscle structure. In contrast, the muscles of Positive group had fewer blue collagen fibers and orderly muscle structure (Fig. 7B). In CMTA group, blue collagen fibers almost disappeared with intact muscle structure. At day 28, no significant improvement was observed in Control and T1DM-ASC groups. Significant muscle repair was observed in Positive group, but collagen fibers still existed. CMTA group had maintained muscle repair, no blue collagen fibers, and intact muscle structure, suggesting that CMTA

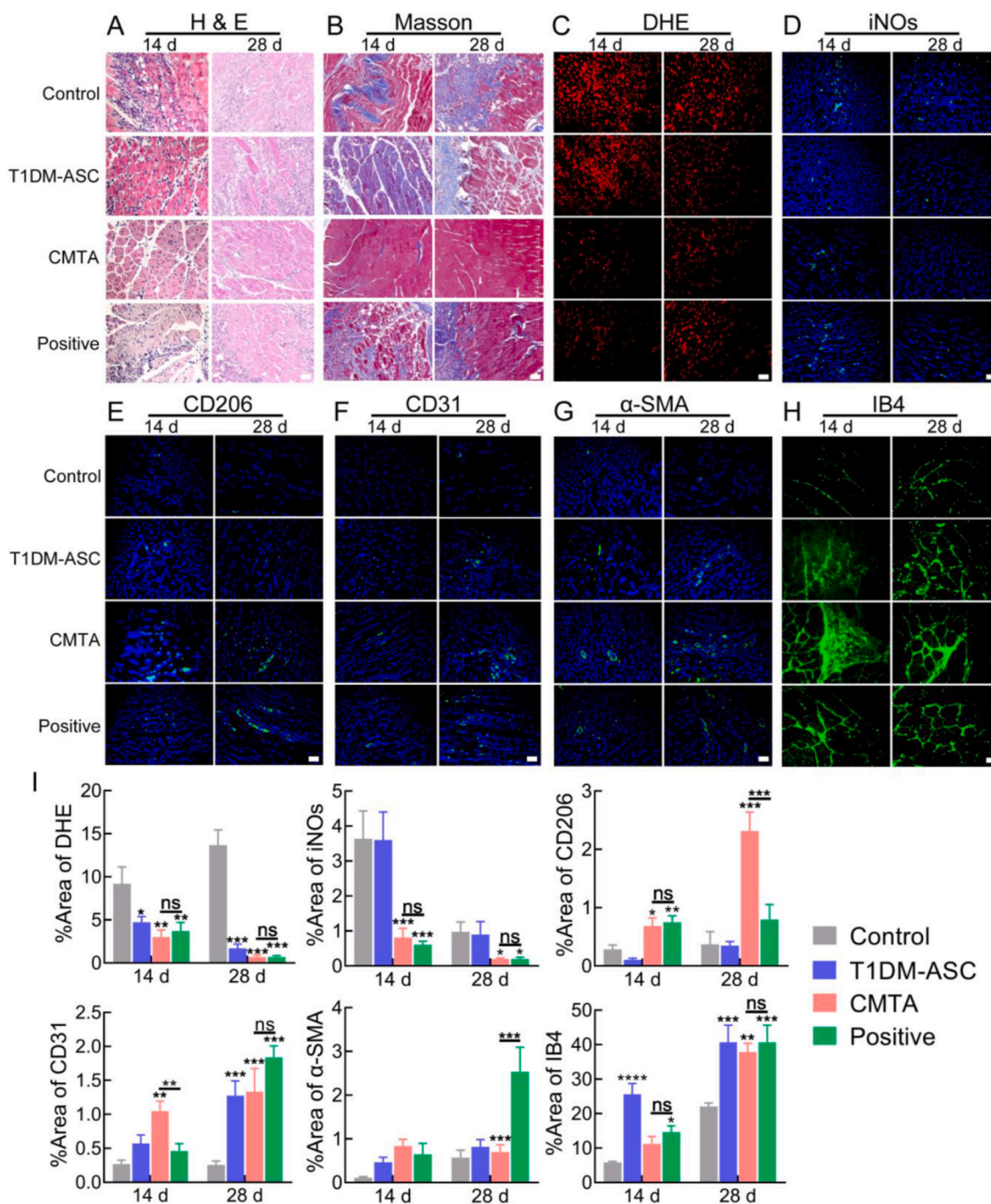


Fig. 7. After Cu-MON treatment, T1DM-ASC showed good therapeutic effects at a smaller dose. (A–H) Representative images of ischemic gastrocnemius after staining with H&E, Masson, DHE, iNOs, CD206, CD31, α -SMA and IB4, Bar = 50 μ m, and (I) their positive area analyzed by Image J software. The data are presented as the mean \pm SEM (n = 3–6, *P < 0.05, **P < 0.01, ***P < 0.001 and ****P < 0.0001).

significantly promoted muscle fiber repair in ischemic hind-limb. In addition, DHE staining was performed to observe ROS levels in gastrocnemius muscle. The ROS levels in the ischemic muscle were all decreased in T1DM-ASC, CMTA, and Positive groups (Fig. 7C, I), suggesting that CMTA improved oxidative stress in the microenvironment. Then, iNOS and CD206 were used to label the levels of M1 and M2 macrophages, respectively. In terms of iNOS-labeled M1 macrophages, the number of positive cells in Control and T1DM-ASC groups was highest at day 14; these groups were followed by the CMTA and Positive groups (Fig. 7D, I). Compared with day 14, at day 28, the number of M1 macrophages decreased in all groups, suggesting the self-repair phenomenon of mice. And CMTA showed an excellent effect in reducing the number of M1 macrophages. Moreover, at day 14, the number of CD206-labeled M2 macrophages in Positive group was significantly higher than that in CMTA group. However, the trend was in the complete opposite direction at day 28, as the level was higher in CMTA group than in Positive group (Fig. 7E, I).

Stable angiogenesis requires coverage of cells in the vessel wall [56]. Angiogenesis of gastrocnemius muscle was visualized by immunofluorescence staining to explore the stability of neovascularization. CD31 and α -SMA were used to observe the levels of endothelial cells and smooth muscle cells. The expression of positive cells was higher in T1DM-ASC, CMTA, and Positive groups than in Control group (Fig. 7F, G, I). This finding suggests that the small-diameter neovascularization was significantly increased in T1DM-ASC, CMTA, and Positive groups, and the coverage of neovascular wall cells was obvious. In particular, CMTA recovered more quickly and stably. Moreover, the number of new blood vessels formed was highest in the CMTA group at day 14, suggesting that CMTA promoted stable angiogenesis. In addition, IB4 was used to identify blood vessels. At day 14, the blood vessels in Control group were tortuous, with a large non-perfusion area and reduced branching of blood vessels. After CMTA treatment, the vessels branched more, but inflammatory cells were still present. As shown in Fig. 7H and I, at day 28, there was no obvious vascular recovery in the control group. After CMTA treatment, there were almost no inflammatory cells, and the vascular network was increased, connected and clear. The vascular networks in T1DM-ASC group and Positive group were fewer and scattered, suggesting that the treatment effect of CMTA was the best.

As shown in Fig. 1K, the expression of VEGF and bFGF was significantly increased in CMTA group. To clearly demonstrate the superiority of CMTA secretion, the T1DM-ASC and CMTA secretions were collected and scatteringly injected into the muscle of mice with critical limb ischemia to observe the therapeutic effect. As expected, CMTA secretions (described below as CMTA-CM) promoted the relaxation of curled feet, improved blood flow recovery, and enhanced motor function compared to the secretions of Control group and T1DM-ASC group (described below as T1DM-ASC-CM) (Supplementary Figs. 20, 21A, B). Notably, there was no statistical difference between CMTA-CM treatment and ND-ASC-CM treatment. Moreover, the levels of IL-6, TNF- α , and IL-1 β were lower in the mouse serum of the T1DM-ASC-CM group, CMTA-CM group and ND-ASC-CM group than that of the control group (Supplementary Fig. 21C). Tissue section staining showed that CMTA-CM reduced inflammatory cell infiltration, collagen fiber infiltration, oxidative stress and the number of M1 macrophages and increased the number of M2 macrophages, thus promoting the vascular network reconstruction (Supplementary Fig. 22). The above results indicate that CMTA showed superior therapeutic effects compared with both cell and secretion treatment than T1DM-ASC. Compared with ND-ASC, CMTA showed comparable or even better therapeutic effects, showing its great potential in angiogenesis and tissue repair. Significantly, the number of cells in CMTA decreased by 85% compared to ND-ASC.

4. Discussion

Impaired angiogenesis and the consequent ischemia of organs and tissues, such as critical limb ischemia (CLI), are a serious peripheral

artery disease. Critical limb ischemia is a severe form of peripheral artery disease that is characterized by impaired angiogenesis and a high risk of subsequent limb loss. It is estimated that the one-year amputation rate of CLI is up to 30% if treated conservatively, and the five-year survival rate is only 25%–50% [57]. In addition, patients with critical limb ischemia often have other diseases, such as hypertension, hyperlipidemia, and diabetes. Among them, diabetic critical limb ischemia is the most intractable due to both large- and microvascular deficits. At present, one patient with diabetes undergoes amputation due to ischemia every 20 s worldwide [58]. The rate of large amputation is 2.14%, and the rate of small amputation is 16.88% [59]. In addition, some patients face reamputations 1–5 times. Thus, diabetic CLI has caused huge clinical and economic burdens, including tens of thousands of lower limb amputations, a dramatic reduction in quality of life and high related costs (approximately \$12, 800 per capita in the United States). Over the past few decades, cytokine therapy [60], gene therapy [61], and cell transplantation therapy [62] have been extensively studied from bench to bedside, however, large controlled studies have shown that they are not as effective as expected in relieving symptoms in CLI patients [63]. There is still no cure for diabetic CLI, and there is an urgent need for innovative ways to expand vascular regeneration to save lives and patients' limbs, thereby improving the overall quality of life. Therefore, in this study, a CLI model was used to evaluate the stemness and functionality of T1DM-ASC enhanced by Cu-MON.

In animal models and clinical trials, it has been established that adipose stem cells are a promising strategy for critical limb ischemia [11,12]. However, patients with diabetes often suffer from microvascular and macrovascular diseases caused by ischemia and hypoxia [19, 20]. Such an environment affects the therapeutic efficacy of ASC. In this study, the lower amounts of VEGF, EGF, and bFGF secreted by T1DM-ASC, which are the three major cytokines mediating the protective effects of ASC [64], may influence the therapeutic effect of T1DM-ASC on tissue repair. Indeed, in our study, the adipogenic and chondrogenic differentiation capacity of T1DM-ASC was less intact than that of ND-ASC, with somewhat elevated intracellular ROS levels. All these results suggested that the presence of diabetes had significant effects on the characteristics and function of T1DM-ASC.

Critical limb ischemic repair is an extremely complex and dynamic process, requiring a wide range of different cells, growth factors, and tissue events, including cell migration, proliferation, angiogenesis, and extracellular matrix deposition [65]. Ischemic repair in patients with diabetes is often significantly delayed, as long-term high glucose levels cause neuropathy and compromised circulation [19,20]. Furthermore, increased expression of inflammatory cytokines, decreased production of growth factors and chemokines, fibroblast proliferation and migration, and decreased angiogenesis and collagen secretion also lead to delayed ischemic repair [66]. Therefore, using biomaterials to regulate the stemness and functionality of T1DM-ASC would be an excellent strategy for diabetic CLI. In our previous study, Cu-MON achieved excellent therapeutic results in diabetic critical limb ischemic mice by regulating redox homeostasis, promoting M2 macrophage polarization, and promoting endothelial repair [25]. In this study, T1DM-ASC and Cu-MON were co-incubated to regulate the stemness and functionality of T1DM-ASC, specifically by promoting M2 macrophage polarization, endothelial cell migration and tube formation, and smooth muscle cell and fibroblast migration and improving the resistance of T1DM-ASC in adverse environments.

Often, the mechanisms by which adipose stem cells regulate ischemic repair in diabetic critical limb ischemia repair involve vasculogenesis, angiogenesis, arteriogenesis, and paracrine effects [67,68]. These four effects have synergistic effects, in which the paracrine effects promote the formation and development of the other three mechanisms and jointly restore the blood supply and oxygen supply of tissues after ischemia [69]. Regulating the paracrine function of T1DM-ASC will be more conducive to promoting ischemic repair. The results of this study indicated that damage to ASC by diabetes was partially reversed by

incubating with Cu-MON. Due to the unique complexity of the paracrine effect, a variety of growth factors and cytokines are involved, and a causal effect cannot be attributed to any single factor or regulatory protein. However, it is likely to be a synergistic effect of a combination factor [46]. Moreover, CMTA promoted the cytokine–cytokine receptor interaction pathway to a greater degree than T1DM-ASC. CMTA up-regulated the protein expression of VEGF, EGF, and bEGF after 2 days of treatment with Cu-MON, suggesting that these ASC have the potential to respond to Cu-MON by stimulating angiogenic factors. Therefore, the treatment of certain angiogenic factor defects and immunomodulatory factor defects by Cu-MON was necessary to reconstruct the cascade of ischemic repair in the lower limbs. In addition, among the top 13 differentially expressed genes, some genes were also expressed in HUVEC, Myoblast, Myofibroblast, and Vascular Smooth Muscle cells, inferring the common role of these cell types. These highly expressed genes have also been shown to positively influence cell functions such as regulating chronic inflammation [34,35], resisting oxidative stress [36, 37], promoting endothelial cell proliferation [38], participating in the recruitment of fibroblasts and endothelial cells [39], and promoting angiogenesis [40,41]. Taken together, these findings suggest that the application of Cu-MON to T1DM-ASC promoted cell migration and angiogenesis and partially recovered the regulated transcriptome after induction by regulating ASC stemness and functionality and positively influencing multiple overall repair processes, including immunomodulation.

Moreover, CMTA was used to treat diabetic critical limb ischemic mice with 80% flow recovery at day 14 after injury. This result was superior to previously reported interventions with similar models [25, 70,71]. Such an intervention was HGF treatment, which is the only recombinant growth factor therapy in Phase 3 clinical trials for CLI. In addition, CMTA secretions also had excellent blood flow recovery effects, reaching 90% blood flow recovery by day 21 after injury. Overall, ischemia repair data based on cell models, transcriptomic analysis, and animal models support our view and suggest that the application of Cu-MON to regulate T1DM-ASC stemness and functionality provide a promising therapeutic solution for diabetic critical limb ischemia. We envision that CMTA have the potential for commercialization and ultimately translation into clinical treatment in patients with diabetic critical limb ischemia. This approach can also be effective in other acute or chronic angiogenesis-dependent diseases, such as skin repair and myocardial ischemia. However, further steps are needed for further research and potential clinical translation. Future studies should focus on employing multiomics approaches to comprehensively map the signaling pathways of CMTA. Furthermore, further studies are needed to determine the indications, application frequency, and appropriate dose levels for different patient populations before CMTA can be used in a clinical setting.

5. Conclusion

In this study, Cu-MON promoted the stemness and functionality of T1DM-ASC. Cu-MON also promoted the interaction and coaction between T1DM-ASC and macrophages, endothelial cells, smooth muscle cells and fibroblasts by regulating the cytokine–cytokine receptor interaction pathway, thus exhibiting an excellent blood flow recovery ability in a diabetic model of critical limb ischemia. In addition, excellent therapeutic effects were achieved with only 15% of the regular cell dose of CMTA, which greatly reduces the cost. Therefore, this approach could provide a new therapeutic option for angiogenesis-dependent diseases.

Notes

The authors declare no competing interests.

CRedit authorship contribution statement

Kaijing Liu: Writing – original draft, Visualization, Methodology, Investigation, Conceptualization. **Ruihao Li:** Writing – original draft, Methodology. **Shusen Wang:** Funding acquisition. **Xue Fu:** Investigation. **Ni Zhu:** Investigation. **Xiaoyu Liang:** Visualization. **Huiyang Li:** Visualization. **Xiaoli Wang:** Writing – original draft, Supervision. **Le Wang:** Supervision, Project administration. **Yongjun Li:** Supervision, Project administration, Funding acquisition. **Jianwu Dai:** Supervision. **Jing Yang:** Writing – review & editing, Supervision, Project administration, Funding acquisition, Conceptualization.

Declaration of competing interest

The authors declare that they have no known competing financial interests or personal relationships that could have appeared to influence the work reported in this paper.

Acknowledgements

National Natural Science Foundation of China (82072080), CAMS Innovation Fund for Medical Sciences (2023-12M-2-008, 2022-12M-3-002, 2021-12M-1-058). This project was supported by Special Program for High-Tech Leader & Teams of Tianjin Government, and Tianjin innovation Promotion Plan Key Innovation Team of Immunoreactive Biomaterials. The authors would like to thank shiyanjia lab (www.shiyanjia.com) for primer synthesis.

Appendix A. Supplementary data

Supplementary data to this article can be found online at <https://doi.org/10.1016/j.bioactmat.2024.03.013>.

Abbreviations

T1DM-ASC	adipose-derived stem cells from type 1 diabetic donors
T2DM-ASC	adipose-derived stem cells from type 2 diabetic donors
ND-ASC	adipose-derived stem cells from non-diabetic donors
Cu-MON	copper-based metal-organic networks
CMTA	T1DM-ASC pretreated with Cu-MON
CM	conditioned medium from T1DM-ASC
Cu-MON-CM	co-culture supernatant of T1DM-ASC and Cu-MON
T1DM-ASC-CM	conditioned medium from T1DM-ASC
CMTA-CM	Cu-MON stimulated T1DM-ASC-conditioned medium
ND-ASC-CM	conditioned medium from ND-ASC

References

- [1] A. Jeyagaran, C.-e. Lu, A. Zbinden, A.L. Birkenfeld, S.Y. Brucker, S.L. Layland, Type 1 diabetes and engineering enhanced islet transplantation, *Adv. Drug Deliv. Rev.* 189 (2022) 114481.
- [2] L. Li, J. Mu, Y. Zhang, C. Zhang, T. Ma, L. Chen, T. Huang, J. Wu, J. Cao, S. Feng, Y. Cai, M. Han, J. Gao, Stimulation by exosomes from hypoxia preconditioned human umbilical vein endothelial cells facilitates mesenchymal stem cells angiogenic function for spinal cord repair, *ACS Nano* 16 (7) (2022) 10811–10823.
- [3] G. Socie, Long-term outcomes after transplantation for acute myelogenous leukemia, *J. Clin. Oncol.* 40 (28) (2022) 3235–3238.
- [4] W. Kim, C.H. Jang, G. Kim, Bone tissue engineering supported by bioprinted cell constructs with endothelial cell spheroids, *Theranostics* 12 (12) (2022) 5404–5417.
- [5] D.M. Hoang, P.T. Pham, T.Q. Bach, A.T.L. Ngo, Q.T. Nguyen, T.T.K. Phan, G. H. Nguyen, P.T.T. Le, V.T. Hoang, N.R. Forsyth, M. Heke, L.T. Nguyen, Stem cell-based therapy for human diseases, *Signal Transduct. Targeted Ther.* 7 (1) (2022) 272.
- [6] P. Manna, S.K. Jain, Hydrogen sulfide and l-cysteine increase phosphatidylinositol 3,4,5-trisphosphate (PIP3) and glucose utilization by inhibiting phosphatase and tensin homolog (PTEN) protein and activating phosphoinositide 3-kinase (PI3K)/Serine/Threonine protein kinase (AKT)/Protein kinase c ζ / λ (PKC ζ / λ) in 3T3L1 adipocytes, *J. Biol. Chem.* 286 (46) (2011) 39848–39859.
- [7] E.K. Shevchenko, P.I. Makarevich, Z.I. Tsokolaeva, M.A. Boldyreva, V.Y. Sysoeva, V.A. Tkachuk, Y.V. Parfyonova, Transplantation of modified human adipose

- derived stromal cells expressing VEGF165 results in more efficient angiogenic response in ischemic skeletal muscle, *J. Transl. Med.* 11 (1) (2013) 138.
- [8] J. Galipeau, L. Sensébé, Mesenchymal stromal cells: clinical challenges and therapeutic opportunities, *Cell Stem Cell* 22 (6) (2018) 824–833.
- [9] M. Qadura, D.C. Terenzi, S. Verma, M. Al-Omran, D.A. Hess, Concise review: cell therapy for critical limb ischemia: an integrated review of preclinical and clinical studies, *Stem Cell* 36 (2) (2018) 161–171.
- [10] J. Leong, Y.-T. Hong, Y.-F. Wu, E. Ko, S. Dvoretzkiy, J.Y. Teo, B.S. Kim, K. Kim, H. Jeon, M. Boppert, Y.Y. Yang, H. Kong, Surface tethering of inflammation-modulatory nanostimulators to stem cells for ischemic muscle repair, *ACS Nano* 14 (5) (2020) 5298–5313.
- [11] M.-L. Kang, H.-S. Kim, J. You, Y.S. Choi, B.-J. Kwon, C.H. Park, W. Baek, M.S. Kim, Y.J. Lee, G.-I. Im, J.-K. Yoon, J.B. Lee, H.-J. Sung, Hydrogel cross-linking-programmed release of nitric oxide regulates source-dependent angiogenic behaviors of human mesenchymal stem cell, *Sci. Adv.* 6 (9) (2020) eay5413.
- [12] G.-J. Jeong, G.-B. Im, T.-J. Lee, S.-W. Kim, H.R. Jeon, D.-H. Lee, S. Baik, C. Pang, T.-H. Kim, D.-I. Kim, Y.C. Jang, S.H. Bhang, Development of a stem cell spheroid-laden patch with high retention at skin wound site, *Bioengineering & Translational Medicine* 7 (2) (2022) e10279.
- [13] W. Srifa, N. Kosaric, A. Amorin, O. Jadi, Y. Park, S. Mantri, J. Camarena, G. C. Gurtner, M. Porteus, Cas9-AAV6-engineered human mesenchymal stromal cells improved cutaneous wound healing in diabetic mice, *Nat. Commun.* 11 (1) (2020) 2470.
- [14] Z. Shirbaghaee, M. Hassani, S. Heidari Keshel, M. Soleimani, Emerging roles of mesenchymal stem cell therapy in patients with critical limb ischemia, *Stem Cell Res. Ther.* 13 (1) (2022) 462.
- [15] L. Bacakova, J. Zarubova, M. Travnickova, J. Musilkova, J. Pajorova, P. Slepicka, N.S. Kasalkova, V. Svorcik, Z. Kolska, H. Motarjemi, M. Molitor, Stem cells: their source, potency and use in regenerative therapies with focus on adipose-derived stem cells – a review, *Biotechnol. Adv.* 36 (4) (2018) 1111–1126.
- [16] F. Jaluvka, P. Ihnat, J. Madaric, A. Vrtkova, J. Janosek, V. Prochazka, Current status of cell-based therapy in patients with critical limb ischemia, *Int. J. Mol. Sci.* (2020).
- [17] V. Capilla-González, J. López-Beas, N. Escacena, Y. Aguilera, A. de la Cuesta, R. Ruiz-Salmerón, F. Martín, A. Hmadcha, B. Soria, PDGF restores the defective phenotype of adipose-derived mesenchymal stromal cells from diabetic patients, *Mol. Ther.* 26 (11) (2018) 2696–2709.
- [18] B. Soria-Juan, N. Escacena, V. Capilla-González, Y. Aguilera, L. Llanos, J.R. Tejedo, F.J. Bedoya, V. Juan, A. De la Cuesta, R. Ruiz-Salmerón, E. Andreu, L. Grochowicz, F. Prósper, F. Sánchez-Guijo, F.S. Lozano, M. Miralles, L. Del Río-Solá, G. Castellanos, J.M. Moraleda, R. Sackstein, M. García-Arraz, D. García-Olmo, F. Martín, A. Hmadcha, B. Soria, C.W.G.N.P. Team, Cost-effective, safe, and personalized cell therapy for critical limb ischemia in type 2 diabetes mellitus, *Front. Immunol.* 10 (2019).
- [19] D. Furman, J. Campisi, E. Verdín, P. Carrera-Bastos, S. Targ, C. Franceschi, L. Ferrucci, D.W. Gilroy, A. Fasano, G.W. Miller, A.H. Miller, A. Mantovani, C. M. Weyand, N. Barzilai, J.J. Goronzy, T.A. Rando, R.B. Effros, A. Lucia, N. Kleinstruwer, G.M. Slavich, Chronic inflammation in the etiology of disease across the life span, *Nat. Med.* 25 (12) (2019) 1822–1832.
- [20] T.V. Rohm, D.T. Meier, J.M. Olefsky, M.Y. Donath, Inflammation in obesity, diabetes, and related disorders, *Immunology* 55 (1) (2022) 31–55.
- [21] L. Wang, L. Zhang, X. Liang, J. Zou, N. Liu, T. Liu, G. Wang, X. Ding, Y. Liu, B. Zhang, R. Liang, S. Wang, Adipose tissue-derived stem cells from type 2 diabetes reveal conservative alterations in multidimensional characteristics, *Int J Stem Cells* 13 (2) (2020) 268–278.
- [22] M. Masee, K. Chinn, J.J. Lim, L. Godwin, C.S. Young, T.J. Koob, Type I and II diabetic adipose-derived stem cells respond in vitro to dehydrated human amnion/chorion membrane allograft treatment by increasing proliferation, migration, and altering cytokine secretion, *Adv. Wound Care* 5 (2) (2015) 43–54.
- [23] R.J.C. Bose, B.J. Kim, Y. Arai, I.-b. Han, J.J. Moon, R. Paulmurugan, H. Park, S.-H. Lee, Bioengineered stem cell membrane functionalized nanocarriers for therapeutic targeting of severe hindlimb ischemia, *Biomaterials* 185 (2018) 360–370.
- [24] A.K.A. Silva, S. Perretta, G. Perrod, L. Pidal, V. Lindner, F. Carn, S. Lemieux, D. Alloyeau, I. Boucenna, P. Menasché, B. Dallemagne, F. Gazeau, C. Wilhelm, C. Cellier, O. Clément, G. Rahmi, Thermoresponsive gel embedded with adipose stem-cell-derived extracellular vesicles promotes esophageal fistula healing in a thermo-actuated delivery strategy, *ACS Nano* 12 (10) (2018) 9800–9814.
- [25] K. Liu, L. Liu, H. Guo, R. Xu, X. Liang, Y. Chen, H. Li, X. Fu, X. Wang, H. Chen, Y. Li, J. Yang, Redox modulatory Cu(II)-Baicalein microflowers prepared in one step effectively promotes therapeutic angiogenesis in diabetic mice, *Adv. Healthcare Mater.* (2022) 2202010 n/a(n/a).
- [26] P.J.A. Cock, C.J. Fields, N. Goto, M.L. Heuer, P.M. Rice, The Sanger FASTQ file format for sequences with quality scores, and the Solexa/Illumina FASTQ variants, *Nucleic Acids Res.* 38 (6) (2010) 1767–1771.
- [27] D. Kim, B. Langmead, S.L. Salzberg, HISAT: a fast spliced aligner with low memory requirements, *Nat. Methods* 12 (4) (2015) 357–360.
- [28] S. Shen, J.W. Park, Z.-x. Lu, L. Lin, M.D. Henry, Y.N. Wu, Q. Zhou, Y. Xing, rMATS: robust and flexible detection of differential alternative splicing from replicate RNA-Seq data, *Proc. Natl. Acad. Sci. USA* 111 (51) (2014) E5593–E5601.
- [29] B. Langmead, S.L. Salzberg, Fast gapped-read alignment with Bowtie 2, *Nat. Methods* 9 (4) (2012) 357–359.
- [30] B. Li, C.N. Dewey, RSEM: accurate transcript quantification from RNA-Seq data with or without a reference genome, *BMC Bioinf.* 12 (1) (2011) 323.
- [31] C. Yang, M. Eleftheriadou, S. Kelaini, T. Morrison, M.V. González, R. Caines, N. Edwards, A. Yacoub, K. Edgar, A. Moez, A. Ivetic, A. Zampetaki, L. Zeng, F. L. Wilkinson, N. Lois, A.W. Stitt, D.J. Grieve, A. Margariti, Targeting QKI-7 in vivo restores endothelial cell function in diabetes, *Nat. Commun.* 11 (1) (2020) 3812.
- [32] H.J. Hwang, Y.-R. Lee, D. Kang, H.C. Lee, H.R. Seo, J.-K. Ryu, Y.-N. Kim, Y.-G. Ko, H.J. Park, J.-S. Lee, Endothelial cells under therapy-induced senescence secrete CXCL11, which increases aggressiveness of breast cancer cells, *Cancer Lett.* 490 (2020) 100–110.
- [33] S. Kawaguchi, H. Sakuraba, H. Kikuchi, N. Numao, T. Asari, H. Hiraga, J. Ding, T. Matsumiya, K. Seya, S. Fukuda, T. Imaizumi, Tryptanthrin suppresses double-stranded RNA-induced CXCL10 expression via inhibiting the phosphorylation of STAT1 in human umbilical vein endothelial cells, *Mol. Immunol.* 129 (2021) 32–38.
- [34] W. Yao, J.L. Rose, W. Wang, S. Seth, H. Jiang, A. Taguchi, J. Liu, L. Yan, A. Kapoor, P. Hou, Z. Chen, Q. Wang, L. Nezi, Z. Xu, J. Yao, B. Hu, P.F. Pettazzoni, I.L. Ho, N. Feng, V. Ramamoorthy, S. Jiang, P. Deng, G.J. Ma, P. Den, Z. Tan, S.X. Zhang, H. Wang, Y.A. Wang, A.K. Deem, J.B. Fleming, A. Carugo, T.P. Hefferman, A. Maitra, A. Viale, H. Ying, S. Hanash, R.A. DePinho, G.F. Draetta, Syndecan 1 is a critical mediator of macropinocytosis in pancreatic cancer, *Nature* 568 (7752) (2019) 410–414.
- [35] J. Di Domizio, C. Belkhdja, P. Chenuet, A. Fries, T. Murray, P.M. Mondéjar, O. Demaria, C. Conrad, B. Homey, S. Werner, D.E. Speiser, B. Ryffel, M. Gilliet, The commensal skin microbiota triggers type I IFN-dependent innate repair responses in injured skin, *Nat. Immunol.* 21 (9) (2020) 1034–1045.
- [36] M.G. Cherian, Y.J. Kang, Metallothionein and liver cell regeneration, *Experimental Biology and Medicine* 231 (2) (2006) 138–144.
- [37] H.G. Kim, M. Huang, Y. Xin, Y. Zhang, X. Zhang, G. Wang, S. Liu, J. Wan, A. R. Ahmadi, Z. Sun, S. Liangpunsakul, X. Xiong, X.C. Dong, The epigenetic regulator SIRT6 protects the liver from alcohol-induced tissue injury by reducing oxidative stress in mice, *J. Hepatol.* 71 (5) (2019) 960–969.
- [38] J.-S. Jang, J.-H. Lee, N.-C. Jung, S.-Y. Choi, S.-Y. Park, J.-Y. Yoo, J.-Y. Song, H. G. Seo, H.S. Lee, D.-S. Lim, Rsad2 is necessary for mouse dendritic cell maturation via the IRF7-mediated signaling pathway, *Cell Death Dis.* 9 (8) (2018) 823.
- [39] A.C. Huen, A. Wells, The beginning of the end: CXCR3 signaling in late-stage wound healing, *Adv. Wound Care* 1 (6) (2012) 244–248.
- [40] S. Zbinden, J. Wang, R. Adenika, M. Schmidt, J.U. Tilan, A.H. Najafi, X. Peng, R. M. Lassance-Soares, M. Iantorno, H. Morsli, L. Gercenshtein, G.J. Jang, S. E. Epstein, M.S. Burnett, Metallothionein enhances angiogenesis and arteriogenesis by modulating smooth muscle cell and macrophage function, *Arterioscler. Thromb. Vasc. Biol.* 30 (3) (2010) 477–482.
- [41] K. Wang, X. Dai, J. He, X. Yan, C. Yang, X. Fan, S. Sun, J. Chen, J. Xu, Z. Deng, J. Fan, X. Yuan, H. Liu, E.C. Carlson, F. Shen, K.A. Wintergerst, D.J. Conklin, P. N. Epstein, C. Lu, Y. Tan, Endothelial overexpression of metallothionein prevents diabetes-induced impairment in ischemia angiogenesis through preservation of HIF-1 α /SDF-1/VEGF signaling in endothelial progenitor cells, *Diabetes* 69 (8) (2020) 1779–1792.
- [42] P. Díaz-Herráez, L. Saludas, S. Pascual-Gil, T. Simón-Yarza, G. Abizanda, F. Prósper, E. Garbayo, M.J. Blanco-Prieto, Transplantation of adipose-derived stem cells combined with neuregulin-microparticles promotes efficient cardiac repair in a rat myocardial infarction model, *J. Contr. Release* 249 (2017) 23–31.
- [43] S. Bachmann, M. Jennwein, M. Bubel, S. Guthörl, T. Pohlemann, M. Oberringer, Interacting adipose-derived stem cells and microvascular endothelial cells provide a beneficial milieu for soft tissue healing, *Mol. Biol. Rep.* 47 (1) (2020) 111–122.
- [44] A.Y. Cheng, A.J. García, Engineering the matrix microenvironment for cell delivery and engraftment for tissue repair, *Curr. Opin. Biotechnol.* 24 (5) (2013) 864–871.
- [45] K. Matsuura, Y. Haraguchi, T. Shimizu, T. Okano, Cell sheet transplantation for heart tissue repair, *J. Contr. Release* 169 (3) (2013) 336–340.
- [46] R.A. Saxton, C.R. Glassman, K.C. Garcia, Emerging principles of cytokine pharmacology and therapeutics, *Nat. Rev. Drug Discov.* (2022).
- [47] C. Khatua, S. Min, H.J. Jung, J.E. Shin, N. Li, J. Jun, H.-W. Liu, G. Bae, H. Choi, M. J. Ko, Y.-S. Jeon, Y.J. Kim, J. Lee, M. Ko, G. Shim, H. Shin, S. Lee, S. Chung, Y. K. Kim, J.-J. Song, V.P. Dravid, H. Kang, In situ magnetic control of macroscale nanoligand density regulates the adhesion and differentiation of stem cells, *Nano Lett.* 20 (6) (2020) 4188–4196.
- [48] T. Kinnaird, E. Stabile, M.S. Burnett, M. Shou, C.W. Lee, S. Barr, S. Fuchs, S. E. Epstein, Local delivery of marrow-derived stromal cells augments collateral perfusion through paracrine mechanisms, *Circulation* 109 (12) (2004) 1543–1549.
- [49] J.D. Newman, R. Anthopoulos, G.B.J. Mancini, S. Bangalore, H.R. Reynolds, D. F. Kunichoff, R. Senior, J. Peteiro, B. Bhargava, P. Garg, J. Escobedo, R. Doerr, T. Mazurek, J. Gonzalez-Juanatey, G. Gajos, C. Briguori, H. Cheng, A. Vertes, S. Mahajan, L.A. Guzman, M. Keltai, A.P. Maggioni, G.W. Stone, J.S. Berger, Y. D. Rosenberg, W.E. Boden, B.R. Chaitman, J.L. Fleg, J.S. Hochman, D.J. Maron, Outcomes of participants with diabetes in the ISCHEMIA trials, *Circulation* 144 (17) (2021) 1380–1395.
- [50] M. Razavi, J. Wang, A.S. Thakor, Localized drug delivery graphene bioscaffolds for cotransplantation of islets and mesenchymal stem cells, *Sci. Adv.* 7(47) eabf9221.
- [51] T.-T. Van Nguyen, N.B. Vu, P. Van Pham, Mesenchymal stem cell transplantation for ischemic diseases: mechanisms and challenges, *Tissue Engineering and Regenerative Medicine* 18 (4) (2021) 587–611.
- [52] Y. Li, W. Liu, F. Liu, Y. Zeng, S. Zuo, S. Feng, C. Qi, B. Wang, X. Yan, A. Khademhosseini, J. Bai, Y. Du, Primed 3D injectable microniches enabling low-dosage cell therapy for critical limb ischemia, *Proc. Natl. Acad. Sci. USA* 111 (37) (2014) 13511–13516.
- [53] J.-Y. Shin, J.-K. Yoon, M.K. Noh, S.H. Bhang, B.-S. Kim, Enhancing therapeutic efficacy and reducing cell dosage in stem cell transplantation therapy for ischemic limb diseases by modifying the cell injection site, *Tissue Eng.* 22 (3–4) (2016) 349–362.

- [54] T. Kochi, Y. Imai, A. Takeda, Y. Watanabe, S. Mori, M. Tachi, T. Kodama, Characterization of the arterial anatomy of the murine hindlimb: functional role in the design and understanding of ischemia models, *PLoS One* 8 (12) (2013) e84047.
- [55] J.A. Beckman, P.A. Schneider, M.S. Conte, Advances in revascularization for peripheral artery disease: revascularization in PAD, *Circ. Res.* 128 (12) (2021) 1885–1912.
- [56] H.-W. Lee, J.H. Shin, M. Simons, Flow goes forward and cells step backward: endothelial migration, *Exp. Mol. Med.* 54 (6) (2022) 711–719.
- [57] Y.-J. Chu, X.-W. Li, P.-H. Wang, J. Xu, H.-J. Sun, M. Ding, J. Jiao, X.-Y. Ji, S.-h. Feng, Clinical outcomes of toe amputation in patients with type 2 diabetes in Tianjin, China, *Int. Wound J.* 13 (2) (2016) 175–181.
- [58] K. Bakker, J. Apelqvist, B.A. Lipsky, J.J. Van Netten, F. on behalf of the International Working Group on the Diabetic, The 2015 IWGDF guidance documents on prevention and management of foot problems in diabetes: development of an evidence-based global consensus, *Diabetes Metabol. Res. Rev.* 32 (S1) (2016) 2–6.
- [59] Y. Jiang, X. Ran, L. Jia, C. Yang, P. Wang, J. Ma, B. Chen, Y. Yu, B. Feng, L. Chen, H. Yin, Z. Cheng, Z. Yan, Y. Yang, F. Liu, Z. Xu, Epidemiology of type 2 diabetic foot problems and predictive factors for amputation in China, *Int. J. Low. Extrem. Wounds* 14 (1) (2015) 19–27.
- [60] Y. Shimizu, K. Kondo, R. Hayashida, K.-i. Sasaki, M. Ohtsuka, Y. Fukumoto, S. Takashima, O. Inoue, S. Usui, M. Takamura, M. Sakuma, T. Inoue, T. Nagata, Y. J. Akashi, Y. Yamada, T. Kato, K. Kuwahara, K. Tateno, Y. Kobayashi, R. Shibata, T. Murohara, A. Kodama, K. Takanari, Y. Kamei, K. Komori, Y. Ishizaki, T. Yoshikawa, K. Kiyokawa, H. Rikimaru, H. Otsuka, T. Kudo, H. Shimomura, Y. Fujimoto, T. Nakayama, H. Kitahara, Y. Kubota, N. Mitsukawa, S. Akita, S. Ebisawa, T.-A.m.t.G. the, Therapeutic angiogenesis for patients with no-option critical limb ischemia by adipose-derived regenerative cells: TACT-ADRC multicenter trial, *Angiogenesis* 25 (4) (2022) 535–546.
- [61] M. Shimamura, H. Nakagami, F. Sanada, R. Morishita, Progress of gene therapy in cardiovascular disease, *Hypertension* 76 (4) (2020) 1038–1044.
- [62] E. Takematsu, M. Massidda, J. Auster, P.-C. Chen, B. Im, S. Srinath, S. Canga, A. Singh, M. Majid, M. Sherman, A. Dunn, A. Graham, P. Martin, A.B. Baker, Transmembrane stem cell factor protein therapeutics enhance revascularization in ischemia without mast cell activation, *Nat. Commun.* 13 (1) (2022) 2497.
- [63] M. Rigato, M. Monami, G.P. Fadini, Autologous cell therapy for peripheral arterial disease, *Circ. Res.* 120 (8) (2017) 1326–1340.
- [64] Y. Han, J. Ren, Y. Bai, X. Pei, Y. Han, Exosomes from hypoxia-treated human adipose-derived mesenchymal stem cells enhance angiogenesis through VEGF/VEGF-R, *Int. J. Biochem. Cell Biol.* 109 (2019) 59–68.
- [65] P. Nowak-Sliwinska, K. Alitalo, E. Allen, A. Anisimov, A.C. Aplin, R. Auerbach, H. G. Augustin, D.O. Bates, J.R. van Beijnum, R.H.F. Bender, G. Bergers, A. Bikfalvi, J. Bischoff, B.C. Böck, P.C. Brooks, F. Bussolino, B. Cakir, P. Carmeliet, D. Castranova, A.M. Cimpean, O. Cleaver, G. Coukos, G.E. Davis, M. De Palma, A. Dimberg, R.P.M. Dings, V. Djonov, A.C. Dudley, N.P. Dufton, S.-M. Fendt, N. Ferrara, M. Fruttiger, D. Fukumura, B. Ghesquière, Y. Gong, R.J. Griffin, A. L. Harris, C.C.W. Hughes, N.W. Hultgren, M.L. Iruela-Arispe, M. Irving, R.K. Jain, R. Kalluri, J. Kalucka, R.S. Kerbel, J. Kitajewski, I. Klaassen, H.K. Kleinmann, P. Koolwijk, E. Kuczynski, B.R. Kwak, K. Marien, J.M. Melero-Martin, L.L. Munn, R. F. Nicosia, A. Noel, J. Nurro, A.-K. Olsson, T.V. Petrova, K. Pietras, R. Pili, J. W. Pollard, M.J. Post, P.H.A. Quax, G.A. Rabinovich, M. Raica, A.M. Randi, D. Ribatti, C. Ruegg, R.O. Schlingemann, S. Schulte-Merker, L.E.H. Smith, J. W. Song, S.A. Stackel, J. Stalin, A.N. Stratman, M. Van de Velde, V.W.M. van Hinsbergh, P.B. Vermeulen, J. Waltenberger, B.M. Weinstein, H. Xin, B. Yektin-Arik, S. Yla-Herttuala, M.C. Yoder, A.W. Griffioen, Consensus guidelines for the use and interpretation of angiogenesis assays, *Angiogenesis* 21 (3) (2018) 425–532.
- [66] D. Baltzis, I. Eleftheriadou, A. Veves, Pathogenesis and treatment of impaired wound healing in diabetes mellitus: new insights, *Adv. Ther.* 31 (8) (2014) 817–836.
- [67] G. Hutchings, K. Janowicz, L. Moncrieff, C. Dompe, E. Strauss, I. Kocherova, M. J. Nawrocki, E. Kruszyna, G. Wasiatycz, P. Antosik, J.A. Shibli, P. Mozdziak, B. Perek, Z. Krasiński, B. Kempisty, M. Nowicki, The proliferation and differentiation of adipose-derived stem cells in neovascularization and angiogenesis, *Int. J. Mol. Sci.* (2020).
- [68] M.W. Majesky, Vascular development, *Arterioscler. Thromb. Vasc. Biol.* 38 (3) (2018) e17–e24.
- [69] Y. Cai, J. Li, C. Jia, Y. He, C. Deng, Therapeutic applications of adipose cell-free derivatives: a review, *Stem Cell Res. Ther.* 11 (1) (2020) 312.
- [70] L. Jia, P. Zheng, H. Wang, L. Kang, H. Wu, X. Fu, VEGF alleviates lower limb ischemia in diabetic mice by altering muscle fiber types, *Exp. Ther. Med.* 23 (4) (2022) 251.
- [71] E. Slobodkina, M. Boldyreva, M. Karagayur, R. Eremichev, N. Alexandrushkina, V. Balabanyan, Z. Akopyan, Y. Parfyonova, V. Tkachuk, P. Makarevich, Therapeutic angiogenesis by a “dynamic duo”: simultaneous expression of HGF and VEGF165 by novel bicistronic plasmid restores blood flow in ischemic skeletal muscle, *Pharmaceutics* (2020).